BILINGUAL PUBLISHING CO.
Pioneer of Global Academics Since 1984

Journal of Metallic Material Research

Volume 5 · Issue 2 · October 2022 | ISSN 2630-5135 (Online)

BILINGUAL PUBLISHING CO.
Pioneer of Global Academics Since 1984

Editor-in-Chief

Prof. Oleg Valentinovich Sobol, Ukraine
Prof. Shouxun Ji, United Kingdom

Editorial Board Members

Shuo Chen, United States
Changrui Wang, China
Madhukar Eknath Navgire, India
Unal Camdali, Turkey
Jitendra Kumar Singh, Korea
Abhay Nanda Srivastva, India
Vivek Patel, India
Bandar Abdulaziz AlMangour, Saudi Arabia
Soumen Maiti, India
Jonathan David Parker, Canada
Samson jerold samuel Chelladurai, India
Akash Deep Sharma, India
Dan Dobrotă, Romania
Asit Kumar Gain, Australia
Dragica Milan Minic, Serbia
Chandan Pandey, India
Mahnaz Mahdavi Shahri, Iran
Deniz Uçar, Turkey
Weidong Song, China
Attoui Aissa, Algeria
Qiaoli Lin, China
Subravel Visvalingam, India
Asaminew Abiyu Cherinet, Ethiopia
Arif Gök, Turkey
Ning Li, China
Fufa Wu, China
Wenchun Jiang, China
Saeed Zeinali Heris, Iran
Vladimir Victorovich Lukov, Russian Federation
Abhishek Ghosh, India
KangHua Chen, China
Pradeep L Menezes, United States
Naushad Ahmad, India
S Selvam, India
Guocheng Zhu, China
Mohamed Kamal ElFawkhry, India
Mohammad Hassan Shirani Bidabadi, China Mohd
Vladimir Mikhailov Yegorovich, Russian Federation
Robin Gupta, India
Sergey Vasilevich Byvaltsev, Russian Federation
Nitin Saini, India
Ramesh Balakrishnan, India
Alexander Evgenievich Barmin, Ukraine
Khitam Abdulhussein Saeed, Malaysia
Paparao Mondi, India
Zbigniew Ranachowski, Poland
Sami ullah Rather, Saudi Arabia
Shengqiang Ma, China
Md Saiful Islam, Bangladesh
Ajay Kumar Choubey, India
Saeed Kakaei, Iran
Hojat Jafari, Iran
Yuhan Liang, United States
Ahmed Wagih, Egypt
Rong Liu, Canada
Francesco Caridi, Italy
Konstanti Viktorovich Ivanov, Russian Federation
Dipak Kumar, India
Americo Scotti, Brazil
Mohsen Vafaeifard, Malaysia
Hülya - Demirören, Turkey
Tahir Mohiuddin Bhat, India
Hamit Özkan Gülsoy, Turkey
Sandhya Dwevedi, India
Sergey Nikolaevich Lezhnev, Kazakhstan
Faysal Fayez Eliyan, Canada
Patrice Berthod, France
Moslem Mansour Lakouraj, Iran
Akhyar - Akhyar, Indonesia
Chih-Chun Hsieh, Taiwan
Lutfiddin Omanivich Olimov, Uzbekistan
Mahmoud Ebrahimi, Iran
Murat Sarıkaya, Turkey
Yaofeng Chang, United States
Mehmet Kaya, Turkey
Meilinda Nurbanasari, Indonesia
Rizk Mostafa Shalaby, Egypt
Anatolii Michailovich Lepikhin, Russian Federation

Volume 5 Issue 2 • October 2022 • ISSN 2630-5135 (Online)

Journal of Metallic Material Research

Editor-in-Chief

Prof. Oleg Valentinovich Sobol

Prof. Shouxun Ji

BILINGUAL PUBLISHING CO.
Pioneer of Global Academics Since 1984

BILINGUAL PUBLISHING CO.
Pioneer of Global Academics Since 1984

Volume 5 | Issue 2 | October 2022 | Page1-38
Journal of Metallic Material Research

Contents

Articles

Review

BILINGUAL PUBLISHING CO.
Pioneer of Global Academics Since 1984

Journal of Metallic Material Research
https://ojs.bilpublishing.com/index.php/jmmr

ARTICLE

As-Cast Microstructures of High Entropy Alloys Designed to Be TaC-Strengthened

Patrice Berthod[1,2*]

1. Faculty of Sciences and Technologies, University of Lorraine, Vandoeuvre-lès-Nancy, 54500, France
2. Institut Jean Lamour, CNRS, Nancy, 54000, France

ARTICLE INFO

Article history
Received: 5 May 2022
Revised: 30 May 2022
Accepted: 1 June 2022
Published Online: 6 June 2022

Keywords:
HEA alloys
TaC carbides
As-cast microstructures
Hardness

ABSTRACT

In this work two new alloys were obtained by extrapolation from a well-known high entropy alloy, the equimolar CoNiFeMnCr one. This was done by the addition of carbon and of tantalum, Ta being one of the strongest MC-former elements. They were produced by conventional casting under inert atmosphere. The obtained microstructures were characterized by X-ray diffraction, metallography, electron microscopy, and energy dispersion spectrometry. Their hardness was also measured by hardness indentation. In parallel, the original CoNiFeMnCr alloy was also synthesized and characterized for comparison. The reference HEA alloy is single-phased with an austenitic structure, while the two {Ta, C}-added alloys are double-phased, with an austenitic matrix and interdendritic script-like TaC carbides. The matrixes of these HEA/TaC alloy are equivalent to an equimolar CoNiFeMnCr alloy to which 2 wt.% Ta is present in solid solution. The presence of the TaC carbides caused a significant increase in hardness which suggests that the HEA/TaC alloys may be mechanically stronger than the HEA reference alloy at high temperature.

1. Introduction

The past decade has seen the appearance of a new generation of alloys interesting for various uses needing high mechanical properties: the "high entropy alloy" principle (HEA). Since some of them can offer good general properties at high temperatures, they may compete with the superalloys which are used for a long time in the aeronautic industry (turbine disks and blades, for instance), power generation (burners, hottest parts of turbines…) and industrial processes working at elevated temperature (tools for shaping molten glasses…) [1-3]. Many HEAs contain in equimolar quantities (or also in various quantities) and with different numbers of metals often belonging to the {Fe, Co, Ni, Cr, Mn} list [4,5]. These five elements constitute a quinary system, the thermodynamic description of which was studied until recently [6,7]. Beside the conventional foundry of equimolar FeCoNiCrMn alloys, different

*Corresponding Author:
Patrice Berthod,
Faculty of Sciences and Technologies, University of Lorraine, Vandoeuvre-lès-Nancy, 54500, France; Institut Jean Lamour, CNRS, Nancy, 54000, France;
Email: patrice.berthod@univ-lorraine.fr

DOI: https://doi.org/10.30564/jmmr.v5i2.4685
Copyright © 2022 by the author(s). Published by Bilingual Publishing Co. This is an open access article under the Creative Commons Attribution-NonCommercial 4.0 International (CC BY-NC 4.0) License. (https://creativecommons.org/licenses/by-nc/4.0/).

ways of elaboration of superalloys were recently applied to HEAs: single crystalline growth [8], additive manufacturing [9] or thin film deposition [10]. Their behaviors in case of extreme conditions of solicitations were also explored, mechanical properties [11,12] or chemical reactivity at high temperature [13]. Evolutions of chemical composition - variation of the Co or Ni content [14] (and even suppression of Co [15] or of Ni [16]) - were tested, and the notion of "Medium Entropy Alloys" has also appeared [17]. Nanoparticles of SiC particles have also started to be introduced in HEAs [18].

The equimolar FeCoNiCrMn alloys are not far from cobalt-based superalloys, strengthened by solid solution, or from the matrix of polycrystalline cobalt-based superalloys with grain boundaries strengthened by carbides. Indeed, these cobalt-based superalloys are generally rich in nickel and in chromium, at least. The contents are not equivalent (50 wt.% Co or a little more, 10 wt.% Ni and 30 wt.% Cr) but one can guess that HEAs involving these elements may usefully contain primary chromium carbides or MC carbides as additional phases. The additional presence of such second phase (and third phase in some cases) is likely to push upwards the mechanical resistance at high temperature of HEAs, the matrix intrinsic strength of which can become no longer sufficient. A particular beneficial effect can be expected from the use of TaC carbides earlier successfully tested in polycrystalline chromia-forming cobalt-based model or industrial alloys [19,20].

The aim of this work is to start investigating the principle of {*in situ* precipitated}-interdendritic script-like MC carbides, by synthetizing several HEA-based alloys in which the formation of MC carbides is promoted by the addition of carbon and of Ta, in quantities having earlier led to MC populations in adequate fractions [19,20]. Checking the reproduction of alloys similar to the model alloys cited above but with a matrix equivalent to a HEA, and characterizing their as-cast microstructures as well as their room temperature hardness, are the objectives of this work.

2. Materials and Methods

The three alloys were prepared by mixing pure elements: Co (centimetric flakes), Ni (millimetric balls), Fe (centimetric flakes), Mn (centimetric flakes) and Cr (centimetric blocks) for the "HEA" alloy, with additionally C (millimetric graphite rods) and Ta (millimetric slugs). The purity of all elements was > 99.9 wt.% (Alfa Aesar and Aldrich). The charges were weighed with accuracy to reach 40 g and the following contents:

- Equimolar CoNiFeCrMn, alloy called "HEA ref.";
- 96 wt.% (CoNiFeCrMn) - 0.25 wt.% C - 3.72 wt.% Ta, alloy called "HEA/TaC1";
- 92 wt.% (CoNiFeCrMn) - 0.50 wt.% C - 7.44 wt.% Ta, alloy called "HEA/TaC2".

Each mix of elements was placed in a copper crucible equipping a high frequency induction furnace (CELES, France; power: 50 kW). This metallic crucible was continuously cooled by circulating water at ambient temperature during the elaboration steps.

After introduction of the mix of pure elements, a silica tube was placed around the crucible and closed to allow the evacuation of the present air, operated by pumping. Crucible and silica tube were surrounded by a water-cooled copper coil in which an alternative current circulated. The frequency of the alternative current was between 100 kHz and 150 kHz, and the applied voltage was between 4 kV and 5 kV, this depending on the alloy. After 3 cycles made of pumping until 4×10^{-5} bars followed by filling by pure Argon, the internal atmosphere was considered as being pure Ar, with a pressure rated at about 400 mbars.

Heating led to the melting of the charges made of pure elements, and the obtained liquid alloy was maintained at the highest reached temperature during fifteen minutes to achieve total melting and chemical homogeneity for the liquid. During the cooling, produced by decreasing the input power/voltage, the alloys started solidifying, and later cooled in solid state. After about 20 minutes to 30 minutes, the obtained ingots were again at room temperature and they were extracted from the crucible.

Each ingot was first embedded in a cold resin mixture (ESCIL, France) to be more easily cut using a metallographic saw to produce a sample with the adequate shape and size to prepare a metallographic sample. The cut part was embedded in the cold {resin + hardener} mixture. The obtained embedded alloy samples were ground by using first #600-grade SiC papers, and second #1200-grade papers. Final polishing was carried out using a textile disk enriched with 1 μm hard particles.

The obtained mirror-like samples were put, one after one, in the chamber of a Scanning Electron Microscope/SEM, model JSM-6010LA (JEOL, Japan). Their microstructures were observed in Back Scattered Electrons mode/BSE (acceleration voltage: 15 kV), at different magnifications. The Image J software was used to measure the surface fractions of the present particles (on three × 1000 SEM/BSE images per alloy). Energy Dispersive Spectrometry was used to control the obtained chemical compositions by full frame analysis (at the × 250 magnification). Additionally, spot analyses were performed on the visible particles to identify them and to specify the chemical composition of the matrix. X-ray diffraction/XRD was

also carried out for all alloys to complete the identification of the present phases. This was done using a D8 Advance diffractometer from Bruker (wavelength of the Kα transition of Cu).

The metallographic samples were also subjected to indentation tests to assess the hardness of all alloys. This was carried out using an automatic indentation machine (PRESI, France), according to the Vickers method. The applied load was 10 kg for all tests. Five indentations were carried out per alloy.

3. Results

3.1 Microstructure and Composition of the "HEA ref." Alloy

X-ray diffraction (XRD) carried out on the reference alloy designed to be CoNiFeMnCr equimolar led to the diffractogram given in Figure 1. This one demonstrates that the alloy is single-phased and contains only a Face Centered Cubic solid solution. This is confirmed by the observation of the microstructure of the metallographic sample using the SEM in BSE mode, illustrated by the SEM/BSE micrograph provided in Figure 2 together with an EDS spectrum showing the peaks of the elements present in the alloy. The alloy effectively appears as single-phased while the EDS results (Table 1 and Table 2) confirm that the alloy is really equimolar.

Table 1. Chemical composition in weight percent of the reference alloy (average and standard deviation calculated from the results of three × 250 full frame areas)

HEA ref. Whole alloy	Wt.% Co	Wt.% Ni	Wt.% Fe	Wt.% Mn	Wt.% Cr	
Average content	19.8	21.4	19.5	19.5	19.8	
Standard deviation	0.2	0.2	0.1	0.0	0.1	

Table 2. Chemical composition in atomic percent of the reference alloy (average and standard deviation calculated from the results of three × 250 full frame areas)

HEA ref. Whole alloy	At.% Co	At.% Ni	At.% Fe	At.% Mn	At.% Cr	
Average content	18.9	20.4	19.5	19.9	21.3	
Standard deviation	0.1	0.2	0.1	0.0	0.1	

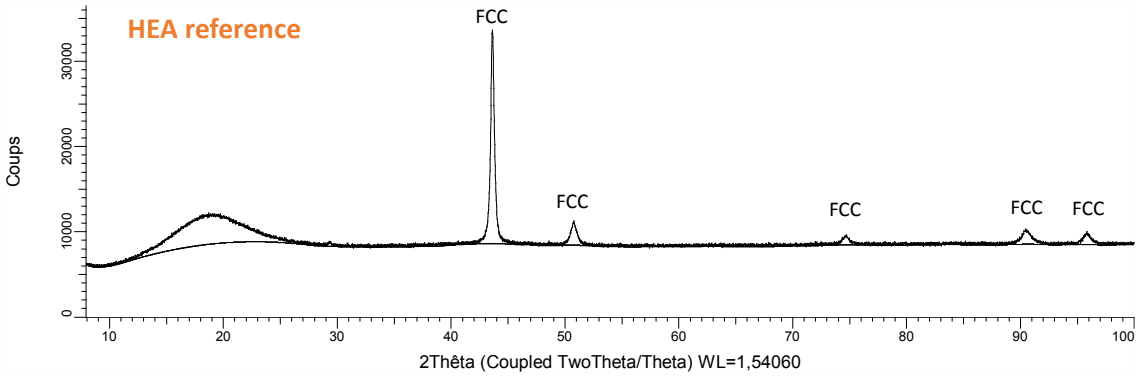

Figure 1. Diffractogram of the HEA reference alloy

(peaks indexed by "FCC": Face Centered Cubic crystalline network of the single phase)

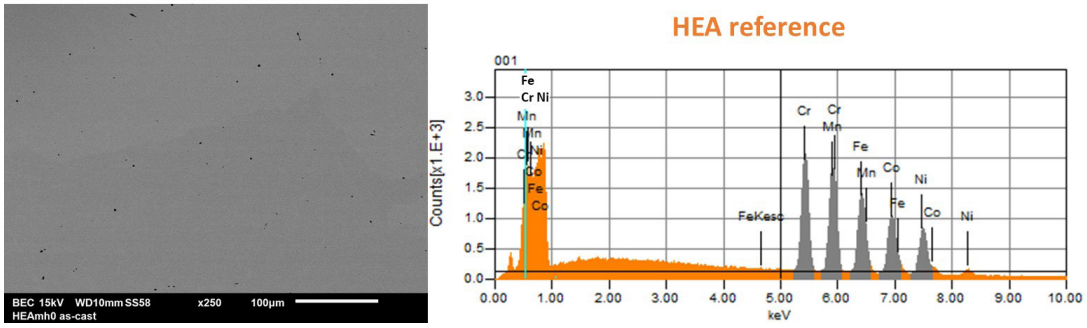

Figure 2. SEM/BSE micrograph of the microstructure of the HEA reference alloy (left) and EDS spectrum acquired on this area (right)

An elemental map was also acquired on the HEA reference alloy to study its chemical homogeneity (Figure 3). It allows observing that all elements are rather homogeneously distributed in the single phase, except manganese which is more present in areas looking as interdendritic spaces.

3.2 Microstructures and Compositions of the {Ta,C}-Containing Alloys

The X-ray diffractograms are acquired on the two alloys resulting from the addition of tantalum and carbon (Figure 4) both contain all the peaks corresponding to the FCC solid solution CoNiFeMnCr already featuring in the diffractogram of the HEA reference alloy (Figure 1). Additional peaks are also present: they correspond to the TaC phase. The microstructures of these two {Ta, C}-containing alloys are illustrated by SEM/BSE micrographs in Figure 5 together with the EDS spectra acquired on these zones. The global chemical compositions of these two alloys measured by full frame EDS analysis on three distinct zones (magnification × 250) and the chemical composition of the matrix measured by spot analysis in three distinct locations, are given in Table 3 for the HEA/TaC1 alloy and in Table 4 for the HEA/TaC2 alloy. Obviously the two alloys each contain at least two phases, including a dendritic matrix. The global chemical compositions are globally well respected.

The microstructure of the HEA/TaC1 alloy is composed of a dendritic matrix and of an interdendritic compound. Observations at higher magnification (Figure 6, left) allow distinguishing two phases in the interdendritic compound. This compound is made of a part of matrix (identified by EDS spot analysis) and of white particles. These ones are TaC carbides, the presence of which was already shown by XRD. The TaC composition was evidenced by spot EDS analysis performed on the coarsest white particles found: almost exclusive presence of Ta and C, and molar equivalence between Ta and C. Due to its interdendritic location and to its constitution in two phases closely imbricated, this compound is certainly of a eutectic nature; it precipitated at the end of solidification with the simultaneous growth of additional matrix and TaC carbides.

Although similar to the HEA/TaC1 one (presence of a dendritic matrix, {matrix + TaC} compound), the microstructure of the HEA/TaC2 alloy presents a particularity since it also contains in addition blocky white particles. EDS spot analysis shows that there are also TaC carbides.

The surface fractions of the TaC phase were measured on three randomly chosen × 1000 SEM/BSE micrographs for the two alloys, using the Image J software, after having rated the threshold to isolate the white TaC from the gray matrix. The HEA/TaC1 alloy contains about 6.4 surf.% of TaC and the HEA/TaC2 contains 11.2 surf.% TaC (average values).

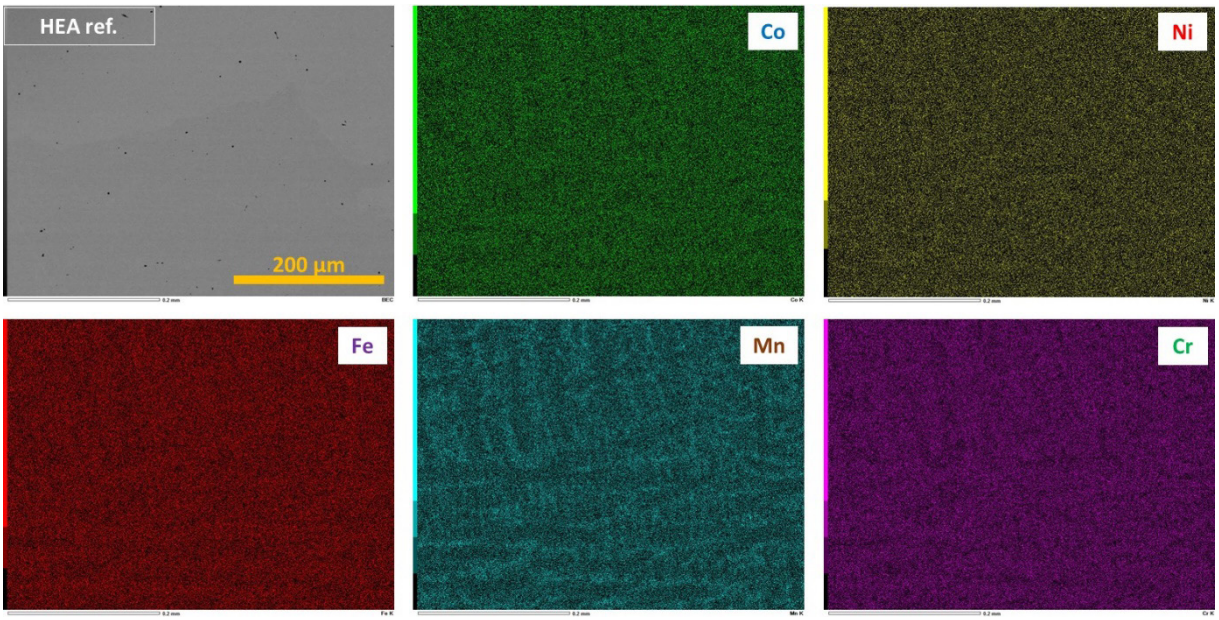

Figure 3. X-maps obtained on the HEA reference

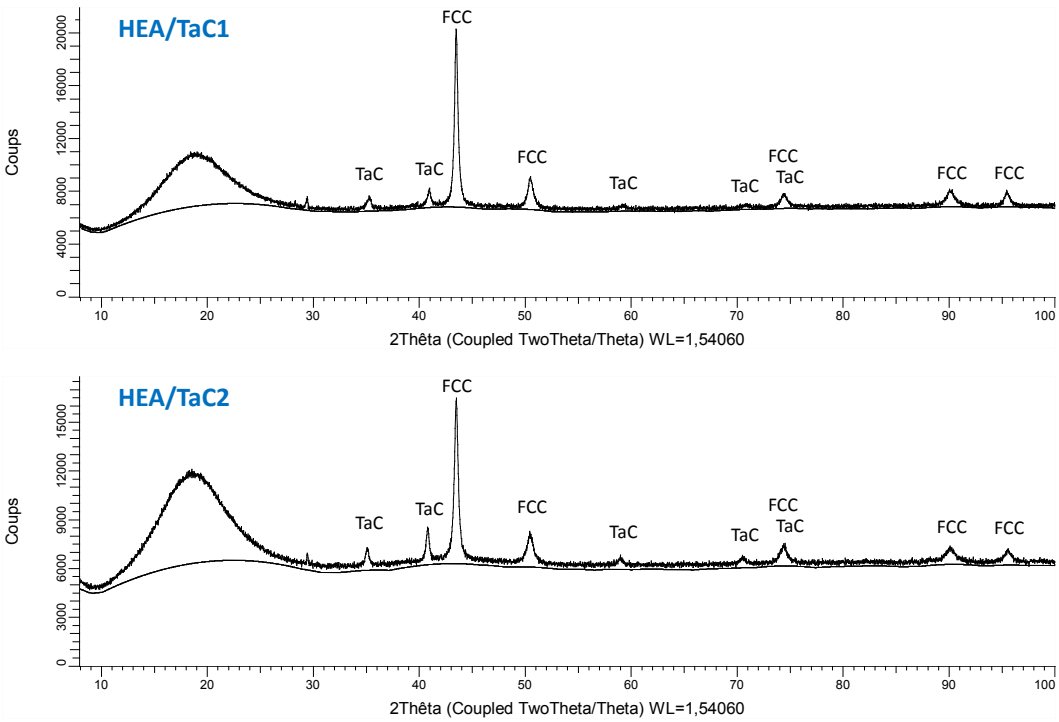

Figure 4. Diffractograms of the HEA/TaC1 (top) and HEA/TaC2 (bottom) alloys

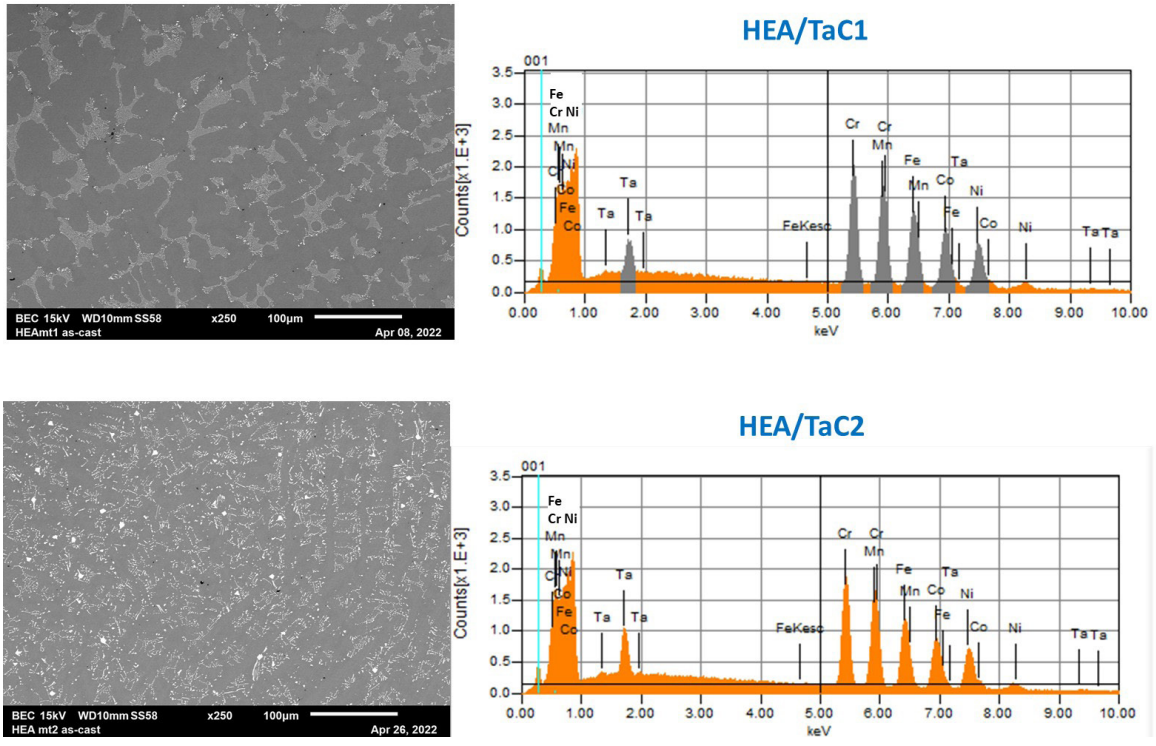

Figure 5. SEM/BSE micrographs of the microstructure of the HEA/TaC1 alloy (top, left) and EDS spectrum acquired on this area (top, right), and of the HEA/TaC2 alloy (bottom left) and the corresponding EDS spectrum (bottom, right)

Table 3. General chemical compositions of the HEA/TaC1 alloy (average and standard deviation calculated from the results of three × 250 full frame areas) and chemical compositions of its matrix (all contents in weight percent, carbon not possible to analyze but supposed to be well respected: 0.25 wt.% C)

HEA/TaC1 Whole alloy	Wt.% Co	Wt.% Ni	Wt.% Fe	Wt.% Mn	Wt.% Cr	Wt.%Ta
Average content	19.3	20.1	18.6	18.3	19.2	4.5
Standard deviation	0.2	0.5	0.5	0.3	0.3	0.4
HEA/TaC1 Matrix	**Wt.% Co**	**Wt.% Ni**	**Wt.% Fe**	**Wt.% Mn**	**Wt.% Cr**	**Wt.%Ta**
Average content	20.5	20.5	20.9	16.7	19.4	2.1
Standard deviation	0.4	0.3	0.9	1.4	0.6	0.1

Table 4. General chemical compositions of the HEA/TaC2 alloy (average and standard deviation calculated from the results of three × 250 full frame areas) and chemical compositions of its matrix (all contents in weight percent, carbon not possible to analyse but supposed to be well respected: 0.5 wt.% C)

HEA/TaC2 Whole alloy	Wt.% Co	Wt.% Ni	Wt.% Fe	Wt.% Mn	Wt.% Cr	Wt.TaC
Average content	18.5	20.0	17.9	18.1	19.1	6.3
Standard deviation	0.5	0.2	0.5	0.2	0.3	0.7
HEA/TaC2 Matrix	**Wt.% Co**	**Wt.% Ni**	**Wt.% Fe**	**Wt.% Mn**	**Wt.% Cr**	**Wt.%TaC**
Average content	18.2	22.8	16.2	22.1	18.9	1.9
Standard deviation	0.5	1.2	2.1	2.0	0.3	0.4

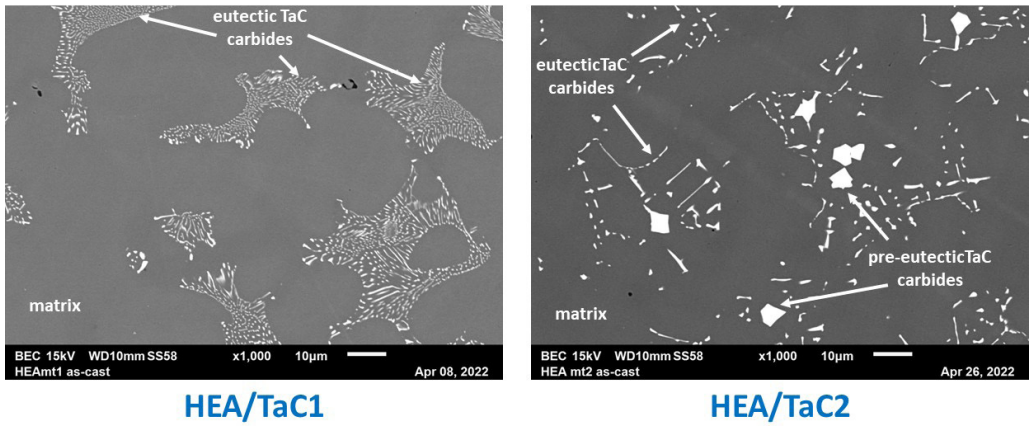

Figure 6. High magnification SEM/BSE micrographs for observation in details of the microstructures of the two {Ta, C}-containing HEA alloys (left: HEA/TaC1, right: HEA/TaC2)

Several EDS spot analyses were also carried out in the matrixes of both alloys (bottom parts of Table 3 and Table 4). Unsurprisingly (since there is only a second phase which is TaC carbide in both alloys), the matrixes are equimolar in Co, Ni Fe, Mn and Cr. But they also contain about 2 wt.% Ta, showing that only a part of tantalum is involved in carbides. A part of carbon is consequently also necessarily present in solid solution in the matrix but, unfortunately, it cannot be analyzed.

One can also notice that the Mn and Fe contents seem varying in the matrix of each alloy. The X-maps presented in Figure 7 effectively evidences in the case of the HEA/TaC1 alloy, slight but real variations in Mn content in its matrix. One encounters again what was observed in the HEA ref. alloy in Figure 3.

3.3 Hardness of the HEA ref. and HEA/TaC Alloys

Per alloy, five indentations were carried out according to the Vickers method, with a 10 kg load. The results, displayed in Table 5, are available for comparison with the hardness of the HEA reference alloy. It clearly appears that the presence of carbides induced a significant increase in hardness.

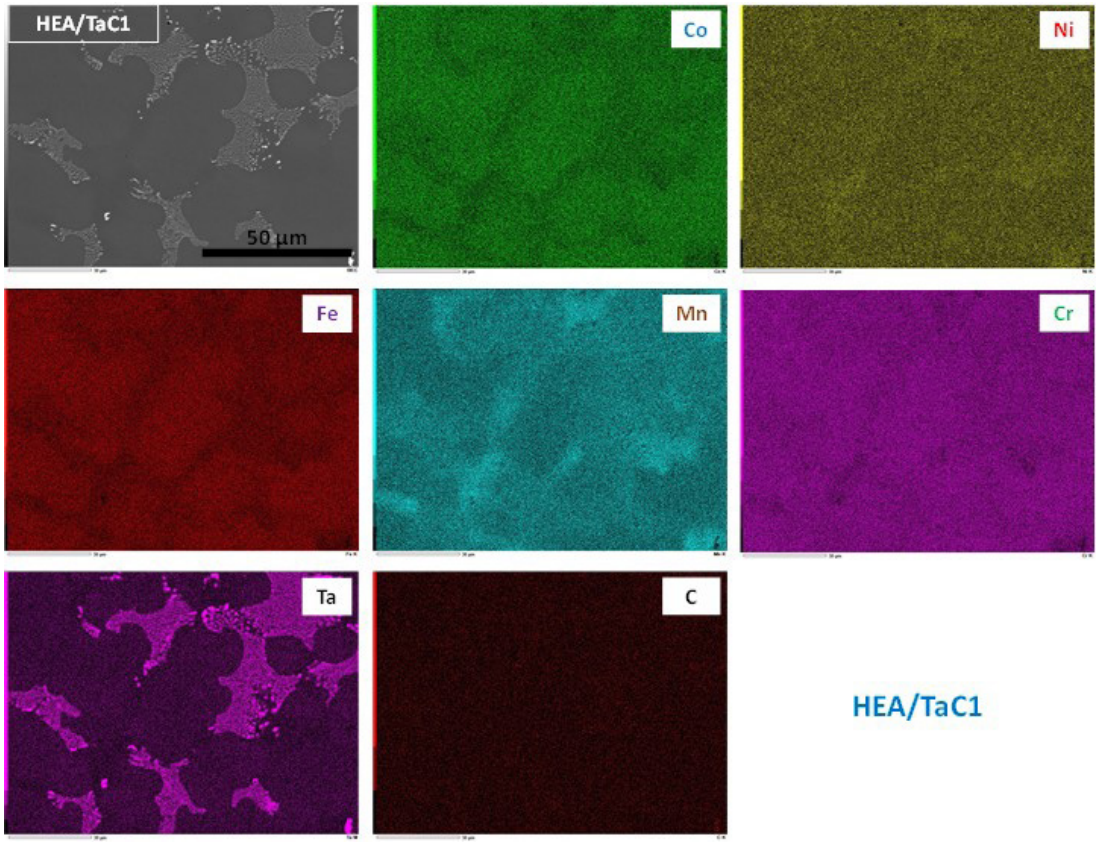

Figure 7. X-maps obtained on the HEA/TaC1 alloy

Table 5. Hardness of the HEA/TaC alloys in comparison with the HEA reference alloy

Vickers 10 kg 5 indent.	HEA ref.	HEA/TaC1	HEA/TaC2
Average content	121	180	194
Standard deviation	2	4	5

4. Discussion

The first alloy to be produced with the apparatus used here (High Frequency Induction furnace, fusion and solidification achieved in a unique water-cooled copper crucible) and the elaboration protocol (all the operating parameters applied here) was the HEA ref. one. It was successfully obtained as a single-phased austenitic alloy, as it is obtained by all researchers working on this type of HEA alloy. The elemental distribution was globally homogeneous, except concerning Mn. The two HEA/TaC alloys themselves presented a matrix globally homogeneous, except Mn again. In their case, the presence of interdendritic particles allowed evidencing that the Mn-enriched zones of the matrix were close to the interdendritic spaces, and thus that Mn was subjected to positive segregation. The knowledge of this not perfect chemical homogeneity of the matrix allows thinking to apply a homogenization heat treatment prior to the use of these alloys, since this small lack of homogeneity can be deleterious for some properties.

The addition of Ta and of C successfully led to an interesting population of carbides. TaC formed at the expense of other types of carbides, notably at the expense of chromium carbides as this previously occurred in earlier alloys fabricated following the same elaboration way and similar protocols (in Ni-30Cr-0.2 or 0.4C-3 or 6Ta [21]). In that way, the 20 wt.% Ni in presence of 20 wt.%Cr is probably compensated by the 20 wt.% Co and 20 wt.% Fe more favorable to the formation of TaC. Indeed, these two last elements did not cause earlier problem of predominance of chromium carbides on TaC carbides in Cr-rich alloys for which they were the base elements [22-24].

As in the earlier studied Cr-rich alloys based on Co [22] or on Fe [23,24], the TaC carbides obtained here have appeared in the last zones to solidify and they are essentially eutectic with close imbrication with matrix, and of the script-like morphology. Good initial interdendrites and intergrains cohesion at high temperature can be thus expected on long time for delaying the transition from secondary state of creep to the tertiary state. It is true that other TaC particles - coarse blocky carbides not mixed with matrix - are present in the HEA/TaC2 alloy, but one can think that they can be not detrimental for the mechanical properties at high temperatures. These blocky TaC are similar to the ones previously observed in cobalt-chromium alloys with high contents in Ta en C (15 wt.% and 1 wt.% C) earlier studied [25]. In these alloys earlier studied, thermodynamic calculations evidence that low C and Ta contents led to the appearance of eutectic TaC carbides only, the dendritic matrix being thus the first solid phase to crystallize from the liquid state. In contrast, higher C and Ta contents induced the pre-eutectic crystallization of a first TaC population instead of the matrix. These pre-eutectic TaC carbides grew, freely in the liquid, with a blocky and angular shape and became the coarse carbides not necessarily located in the interdendritic spaces observed in the metallographic samples. The origin of the blocky carbides observed in the HEA/TaC2 alloy is certainly the same: moving from {0.25 wt.% C, 3.7 wt.% Ta} to {0.50 wt.% C, 7.4 wt.% Ta} obviously induced here too change of location of the alloy from one side of the eutectic valley to the other side, with as consequence a solidification of first TaC and second TaC & matrix, instead a solidification of first matrix and second TaC & matrix. By comparison with these earlier studied cobalt-based alloys, the replacement of a great part of cobalt by new elements to achieve equal proportions in Co, Ni, Fe, Cr and Mn, has obviously caused a displacement of the eutectic valley toward lower tantalum and carbon contents.

To speak again about the matrix, this one is not really an equimolar alloy since it contains also 2 wt.% Ta. This is the typical Ta content in the matrix of Cr-rich Co-based alloys containing 0.2C-3Ta or 0.4C-6Ta (wt.%) [22] (and twice the one in the Cr-rich Fe-based alloys with the same C and Ta contents [23], or half the one in the Cr-rich Fe-based alloys with the same C and Ta contents [21]). The presence of Ta in solid solution in the matrix did not change its single-phase state and it may possibly bring an additional strengthening.

Concerning the properties of these TaC-strengthened alloys at high temperature, an ongoing study has brought first results of microstructure behavior. They are illustrated in Figure 8. After 50 h at 1100 °C, no start of local melting was detected. Furthermore, the TaC carbides population has not significantly changed. The script-like shape of the eutectic carbides is kept, despite a limited fragmentation and the pre-eutectic blocky carbides of the HEA/TaC2 alloy are not affected. There is another modification which is interesting to notice: the precipitation of fine carbides from the Ta and C initially present in solid solution in the matrixes of the as-cast alloys. This is a potential source of additional strengthening which can be useful during the steady state of creep deformation (secondary step of creep). These secondary TaC are more numerous in the HEA/TaC1 alloy than in the HEA/TaC2 alloy. In this second alloy, the higher density of primary TaC led Ta and C diffusing towards the neighbor carbides to precipitate on their surfaces. The contribution of fine dispersed TaC carbides will be thus more useful for the HEA/TaC1 alloy than for the other alloy. Creep tests are scheduled on these HEA/TaC1 and HEA/TaC2 alloys to assess the progress

in strength at high temperature due to these TaC carbides added to the HEA reference alloy.

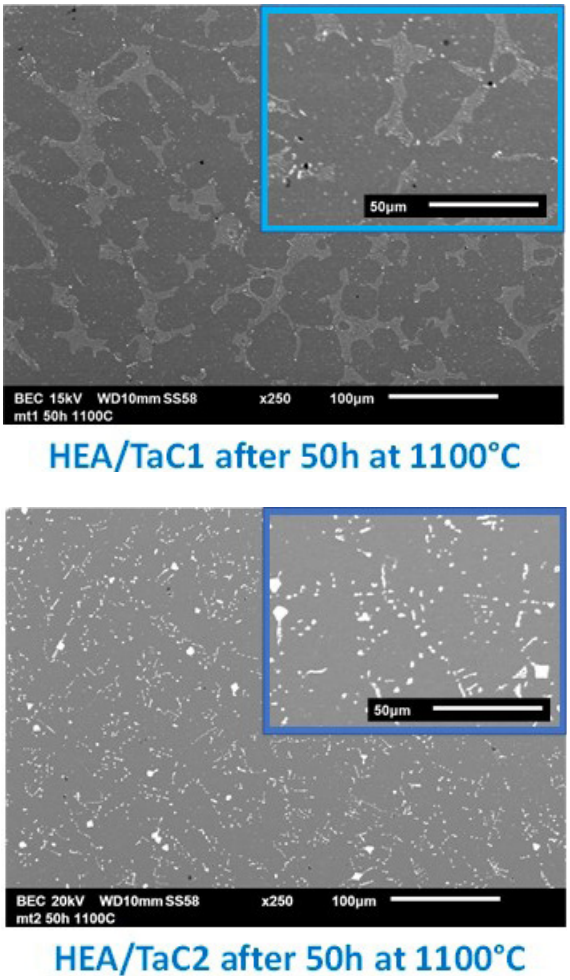

Figure 8. Microstructures of the two HEA/TaC1 (left) and HEA/TaC2 (right) alloys after 50 hours at 1100 °C (SEM/BSE at the × 250 magnification and at × 500 in the top right corners).

5. Conclusions

The as-cast microstructures obtained for the new alloys resulting from the addition of Ta and C to an equimolar CoNiFeMnCr HEA alloy are thus composed of a matrix similar to a HEA alloy, despite the presence of Ta (and C) in solid solution in proportion much lower than the first five elements, and of interdendritic TaC carbides forming a eutectic compound with the peripherical parts of the matrix dendrites. The combination of these two phases can be potentially very interesting, knowing the good properties of equimolar CoNiFeMnCr alloys (furthermore possibly enhanced by Ta in solid solution) and the script-like TaC carbides which have earlier demonstrated their beneficial effect for the creep resistance of Cr-rich Co-based superalloys. Now, the morphological sustainability of the script-like TaC carbides on long term at high temperature needs to be tested, and the mechanical properties are to be tested in hot conditions, by creep tests for instance. Another important point to check is the behavior of these HEA/TaC alloys in oxidation at high temperature. This one risks to be not sufficient because of the rather low chromium content to which the equimolar criterion led. These investigations of the microstructure, mechanical and oxidation properties at high temperature are being done in new ongoing studies.

Author Contributions

This present study is the own work of the single author.

Conflict of Interest

There is no conflict of interest for this work.

Funding

This research received no external funding.

Acknowledgments

To Ghouti Medjahdi, member of the CC X-Gamma service of the Jean Lamour Institute, for his help for the X-ray diffraction runs,

To Erwan Etienne, member of the CC 3M service of the Jean Lamour Institute, for his technical help for the indentation tests.

References

[1] Chester, T.S., Hagel, W.C., 1972. The Superalloys-Vital High Temperature Gas Turbine Materials for Aerospace and Industrial Power. John Wiley & Sons: New York.

[2] Sims, C.T., Stoloff, N.S., Hagel, W.C., 1987. Superalloys II. High: Temperature materials for aerospace and industrial power. John Wiley & Sons: New York.

[3] Kracke, A., Allvac, A., 2010. Superalloys, the most successful alloy system of modern times-past, present and future. Proceedings of the 7th International Symposium on Superalloy. 718, 13-50.

[4] Liu, S.F., Wu, Y., Wang, H.T., et al., 2018. Stacking fault energy of face-centered-cubic high entropy alloys. Intermetallics. 93, 269-273.
DOI: http://dx.doi.org/10.1016/j.intermet.2017.10.004

[5] Ferrari, A., Körmann, F., 2020. Surface segregation in Cr-Mn-Fe-Co-Ni high entropy alloys. Applied Surface Science. 533, 147471.
DOI: https://doi.org/10.1016/j.apsusc.2020.147471

[6] Wilson, P., Field, R., Kaufman, M., 2016. The use of

diffusion multiples to examine the compositional dependence of phase stability and hardness of the Co-Cr-Fe-Mn-Ni high entropy alloy system. Intermetallics. 75, 15-24.
DOI: http://dx.doi.org/10.1016/j.intermet.2016.04.007

[7] Do, H.S., Choi, W.M., Lee, B.J., 2022. A thermodynamic description for the Co-Cr-Fe-Mn-Ni system. Metals and Corrosion. 57, 1373-1389. https://link.springer.com/article/10.1007/s10853-021-06604-8.

[8] Kawamura, M., Asakura, M., Okamoto, N.L., et al., 2021. Plastic deformation of single crystals of the equiatomic Cr−Mn−Fe−Co−Ni high-entropy alloy in tension and compression from 10 K to 1273 K. Acta Materialia. 203, 116454.
DOI: https://doi.org/10.1016/j.actamat.2020.10.073

[9] Osintsev, K., Konovalov, S., Zaguliaev, D., et al., 2022. Investigation of Co-Cr-Fe-Mn-Ni non-equiatomic high-entropy alloy fabricated by wire arc additive manufacturing. Metals. 12, 197.
DOI: https://doi.org/10.3390/met12020197

[10] Hu, M., Cao, Q.P., Wang, X.D., et al., 2022. Tuning nanostructure and mechanical property of Fe−Co−Ni−Cr−Mn high-entropy alloy thin films by substrate temperature. Metals. 12, 197.
DOI: https://doi.org/10.1016/j.mtnano.2021.100130

[11] Mehranpour, M.S., Shahmir, H., Nili-ahmadabadi, M., 2021. Precipitation kinetics in heavily deformed CoCrFeNiMn high entropy alloy. Materials Letters. 288, 129359.
DOI: https://doi.org/10.1016/j.matlet.2021.129359

[12] Xiao, H., Zeng, Q., Xia, L., et al., 2022. Hydrogen-assisted fatigue crack propagation behavior of equiatomic Co-Cr-Fe-Mn-Ni high-entropy alloy. Materials and Corrosion. 73, 550-557.
DOI: https://doi.org/10.1002/maco.202112866

[13] Kim, Y.K., Joo, Y.A., Kim, H.S., et al., 2018. High temperature oxidation behavior of Cr-Mn-Fe-Co-Ni high entropy alloy. Intermetallics. 98, 45-53.
DOI: https://doi.org/10.1016/j.intermet.2018.04.006

[14] Zhu, Z.G., Ma, K.H., Yang, X., et al., 2017. Annealing effect on the phase stability and mechanical properties of (FeNiCrMn)(100-x)Cox high entropy alloys. Journal of Alloys and Compounds. 695, 2945-2950.
DOI: http://dx.doi.org/10.1016/j.jallcom.2016.11.376

[15] Dong, J., Feng, X., Hao, X., et al., 2021. The environmental degradation behavior of FeNiMnCr high entropy alloy in high temperature hydrogenated water. Scripta Materialia. 204, 114127.
DOI: https://doi.org/10.1016/j.scriptamat.2021.114127

[16] Zhang, C., Zhang, F., Jin, K., et al., 2017. Understanding of the elemental diffusion behavior in concentrated solid solution alloys. Journal of Phase Equilibria and Diffusion. 38, 434-444.
DOI: https://doi.org/10.1007/s11669-017-0580-5

[17] Bracq, G., Laurent-Brocq, M., Varvenne, C., et al., 2019. Combining experiments and modeling to explore the solid solution strengthening of high and medium entropy alloys. Acta Materialia. 177, 266-279.
DOI: https://doi.org/10.1016/j.actamat.2019.06.050

[18] Szklarza, Z., Lekki, J., Bobrowski, P., et al., 2018. The effect of SiC nanoparticles addition on the electrochemical response of mechanically alloyed CoCrFeMnNi high entropy alloy. Materials Chemistry and Physics. 215, 385-392.
DOI: https://doi.org/10.1016/j.matchemphys.2018.05.056

[19] Berthod, P., Bernard, J.L., Liébaut, C., 2001. Cobalt-chromium alloy for spinner cups in manufacture of mineral wool from silicate glass. International Patent, PCT International Applications. WO 2001090429 A1 20011129.

[20] Michon, S., Aranda, L., Berthod, P., et al., 2004. High temperature evolution of the microstructure of a cast cobalt base superalloy-Consequences on its thermomechanical properties. Metallurgical Science and Technology. 101, 651-662.
DOI: https://doi.org/10.1051/metal:2004116

[21] Berthod, P., Aranda, L., Vébert, C., et al., 2004. Experimental and thermodynamic study of the high temperature microstructure of tantalum containing nickel-based alloys. Calphad. 28, 159-166.
DOI: https://doi.org/10.1016/j.calphad.2004.07.005

[22] Michon, S., Berthod, P., Aranda, L., et al., 2003. Application of thermodynamic calculations to study high temperature behavior of TaC-strengthened Co-base superalloys. Calphad. 27, 289-294.
DOI: https://doi.org/10.1016/j.calphad.2003.12.003

[23] Berthod, P., Hamini, Y., Aranda, L., et al., 2007. Experimental and thermodynamic study of tantalum-containing iron-based alloys reinforced by carbides: Part I — Case of (Fe, Cr)-based ferritic steels. Calphad. 31, 351-360.
DOI: https://doi.org/10.1016/j.calphad.2007.01.007

[24] Berthod, P., Aranda, L., Hamini, Y., et al., 2007. Experimental and thermodynamic study of tantalum-containing iron-based alloys reinforced by carbides: Part II — Case of (Fe, Ni, Cr)-base austenitic steels. Calphad. 31, 361-369.
DOI: https://doi.org/10.1016/j.calphad.2007.01.008

[25] Berthod, P., Corona, L., 2017. Thermodynamic and experimental study of 30 wt-%Cr-containing {Co, Fe or Ni}-based alloys with very high contents in Ta and C. Canadian Metallurgical Quarterly. 56, 113-122.
DOI: http://dx.doi.org/10.1080/00084433.2016.1267298

BILINGUAL PUBLISHING CO.
Pioneer of Global Academics Since 1984

Journal of Metallic Material Research
https://ojs.bilpublishing.com/index.php/jmmr

ARTICLE

Spatial Investigation of Nilüfer Stream Arsenic Pollution in Previous and Post COVID-19 Pandemic and Evaluation of Health Risks for Adult People

Aslıhan Katip*

Faculty of Engineering, Department of Environmental Engineering, Bursa Uludag University, Bursa, 16059, Turkey

ARTICLE INFO

Article history
Received: 1 May 2022
Revised: 27 July 2022
Accepted: 28 July 2022
Published Online: 23 August 2022

Keywords:
Arsenic pollution
COVID-19
Human health risk
Hazard quotient
Nilüfer stream

ABSTRACT

This study was carried out in Nilüfer Stream in Bursa City, where intensive industrial, agricultural and mining activities are existed. The temporal and spatial variation of arsenic was evaluated by examining its concentrations between March 2015 and December 2021. Values between March 2015 and December 2019 were evaluated as pre-pandemic, and values between March 2020 and December 2021 were evaluated as post-pandemic. The results were compared with national and international standards and the chronic and cancer risks were calculated for adults. When the 7-year general averages were examined, it was seen that the highest concentration was 0.0256 mg/L at the 8th Station, and the lowest concentration was 0.0182 mg/L at the 1st Station. The reason why the highest value is at the 8th station was that the wastewater of Nilüfer and Bursa Organized Industrial Zones was discharged to Bursa West Wastewater Treatment Plant before this station. After the pandemic the raises in concentrations were observed at all stations, except for the 3rd Station. This shows that the pollution load had increased in general during the pandemic. However, it was estimated that there was a decrease in the pollution load of the industrial wastewater coming to the 3rd Station, which was located after the Eastern Wastewater Treatment Plant of the City. It was observed that all stations examined were higher than drinking water standards and lower than irrigation water standards according to WHO and Turkish National Standards. All measuring stations were greater than 1 of the hazard quotient (HQ) values. In terms of human consumption risk, all stations had a chronic and carcinogenic risk according to the values before and after the pandemic. After the pandemic conditions, the HQ order of the stations was 8>10>7>9>2>6>4>1>3. In general, post-pandemic HQ values had generally increased and the risk of cancer had increased.

*Corresponding Author:
Aslıhan Katip,
Faculty of Engineering, Department of Environmental Engineering, Bursa Uludag University, Bursa, 16059, Turkey;
Email: aballi@uludag.edu.tr

DOI: https://doi.org/10.30564/jmmr.v5i2.4741
Copyright © 2022 by the author(s). Published by Bilingual Publishing Co. This is an open access article under the Creative Commons Attribution-NonCommercial 4.0 International (CC BY-NC 4.0) License. (https://creativecommons.org/licenses/by-nc/4.0/).

1. Introduction

Arsenic occurs naturally in the earth's crust and is an element classified as a semi-metal or metalloid. Arsenic could enter waters from pesticides and phosphate fertilizers, mine drainage, oxidation of arsenic-containing sulfide minerals, reduction of arsenic-bearing iron and manganese oxides, discharges of geothermal waters and power plants, improper production, use and disposal of arsenic-containing products [1,2]. Industrial productions containing arsenic include wood, timber preservation, cosmetics, paint enterprises, pharmaceutical industry, herbicide industry, semiconductor material production, leather, glass production, medical uses, paper and pulp production, and cement enterprises. In addition, copper, nickel, gold mining and ore disposal operations, agricultural practices, use of fossil fuels, landfill leachate are among the anthropogenic sources of arsenic [3,4].

In the report titled "Human Development Report 2006 on the Verge of Scarcity: Power, Poverty and the Global Water Crisis" prepared by the United Nations Development Program, Turkey had been shown among the countries with the possibility of arsenic contamination [3]. High levels of arsenic had also been detected in Bursa and its environs, as well as in Balıkesir and Uşak [5,6]. The Nilüfer Stream, which passes through Bursa, where the textile, automotive, metal and chemical industries were intense, agricultural production and mining was carried out, and which was the 4th largest city of Turkey, is under intense pressure in terms of metal pollution [7-9]. There was Emet and Orhaneli Stream within the borders of Bursa City. In the Uluabat Lake Basin formed by the Emet and Orhaeli Streams, there were Keles Lignites Enterprise, Tunçbilek Coal Enterprise, Tunçbilek Thermal Power Plant and Emet Colemanite enterprises on the Emet Stream. It was stated in the literature that the colemanites of the region contain arsenic in the form of orpiment and realgar [10]. It was known that mineralized coal types were rich in toxic trace elements such as arsenic, mercury, antimony, and thallium. Arsenic was mixed into the waters in Uluabat Lake and its Basin, where mining was carried out intensively [10]. The 5 wastewater treatment plants located in the Nilüfer Stream Basin discharged the treated industrial and domestic wastewater to the Stream [8]. It was thought that the use of herbicides containing arsenic compounds in Bursa, which was an important agricultural center in Turkey, causes soil and water pollution [11].

Within the scope of this study, the variation of As pollution between the years 2015-2021 at the measurement stations on the side and main branches of the Nilüfer Stream was investigated. Also, it was aimed to observe the effects of the COVID-19 pandemic on As pollution and to examine the concentration trends in the last 7 years. This study was scientifically original because it was shown the effect of the COVID-19 pandemic on As pollution.

2. Materials and Methods

2.1 Study Area

Nilüfer stream which arises from the border of Bursa city served as an important water supply for the city and reaches the sea after a long flow in the basin. The Nilüfer stream had been exploited to support agriculture and the public water supply. The major sources of pollutants of Nilüfer stream come from point sources which were mainly composed of treated wastewater discharges from organized industrial districts and municipal sewage treatment plants. There were 5 large wastewater treatment plants in the Nilüfer Stream Basin. Two of them (Demirtaş and Bursa Organized Industrial Zones Wastewater Treatment Plant) had a completely industrial wastewater characterization, while the Eastern, Western and Green Environment Wastewater Treatment Plants had domestic and industrial characterization. Also, non-point sources were mainly composed of surface run-off from agricultural areas [7].

In Bursa City, apart from textile, automotive, metal, and chemical industry, wastes arising from the processing of many marble quarries, tungsten, lignite, boron, magnesite, zinc, asbestos, chromium, and olivine ores were found in the basin. In addition, there was 1 coal-fired thermal power plant in the province [12].

Samples were taken from 10 different points, upstream and downstream of the Nilüfer Stream, before and after the wastewater treatment plants. The locations of the measuring stations were given in Table 1 and Figure 1.

Table 1. Locations of the measuring stations

Station No	Location
1	On Nilüfer Stream, Gümüştepe Locality
2	On Deliçay Creek, Before Discharge of East wastewater treatment plant
3	On Deliçay Creek, After Discharge of East wastewater treatment plant
4	On Nilüfer Stream, After Deliçay Creek Mixture
5	İsmetiye Stream
6	On Nilüfer Stream, After Dosab Wastewater Treatment Plant Discharged
7	On Ayvalı Creek Before West Wastewater Treatment Plant Discarharge
8	On Ayvalı Creek, After West Wastewater Treatment Plant Discharge
9	On Hasanağa Creek
10	On Nilüfer Stream, After Hasanağa Creek Mixture

2.2 Laboratory Analyses

Water samples were collected from midstream at a depth of 15 cm ~ 20 cm in 1000 mL polyethylene bottles, which had previously been cleaned by soaking in 10% nitric acid and rinsed with distilled water. At the sampling site, the bottles were rinsed twice with the water to be sampled prior to filling. The water samples were acidified on site to a pH less than 2 with 5 mL of analytical grade concentrated HNO_3. After collection the samples were placed in coolers with ice bags while being transported to the laboratory and kept at about 4 °C until being analyzed [8,13]. Grab samples were collected in dry weather conditions from the 10 measuring stations seasonaly (March, June, September, and December) between 2015 and 2021.

Water samples were implemented digesting process via a CEM MARS-5 model microwave instrument. A 40 mL sample was placed into the cell and then 6 mL of HNO_3 (65% analytical grade) and 4 mL of HCl (37% analytical grade) were added to the cell. 180 psi pressure and 160 °C temperature was applied for 20 minutes to the cell. After cooling 30 minutes to room temperature samples transferred into a 100 mL flask. The digested samples were filled with distilled water to the 100 mL mark, and used in the ICP-AES (Vista MPX, Varian) analysis. The standard calibration solutions were prepared at concentrations of 0.05 mg/L, 0.1 mg/L, 0.25 mg/L, 0.5 mg/L, and 1 mg/L. For higher than 1 mg/L of samples, calibration solution concentrations were prepared at 1 mg/L, 2 mg/L, 5 mg/L, and 10 mg/L. The blanks were done by concentrated 5% HNO_3 into ultrapure water. Quality control was performed with certified liquid samples (multi-elements standard, catalogue number 900-Q30-002, lot number SC0019251, SCP Science, Lasalle, Quebec) to provide the accuracy of the measurements. Quantification limit was 5 µg/L for As. Certified liquid samples were used to check the analytical accuracy, which ranged between 1% and 10%. All reagents used were of analytical grade or better [13].

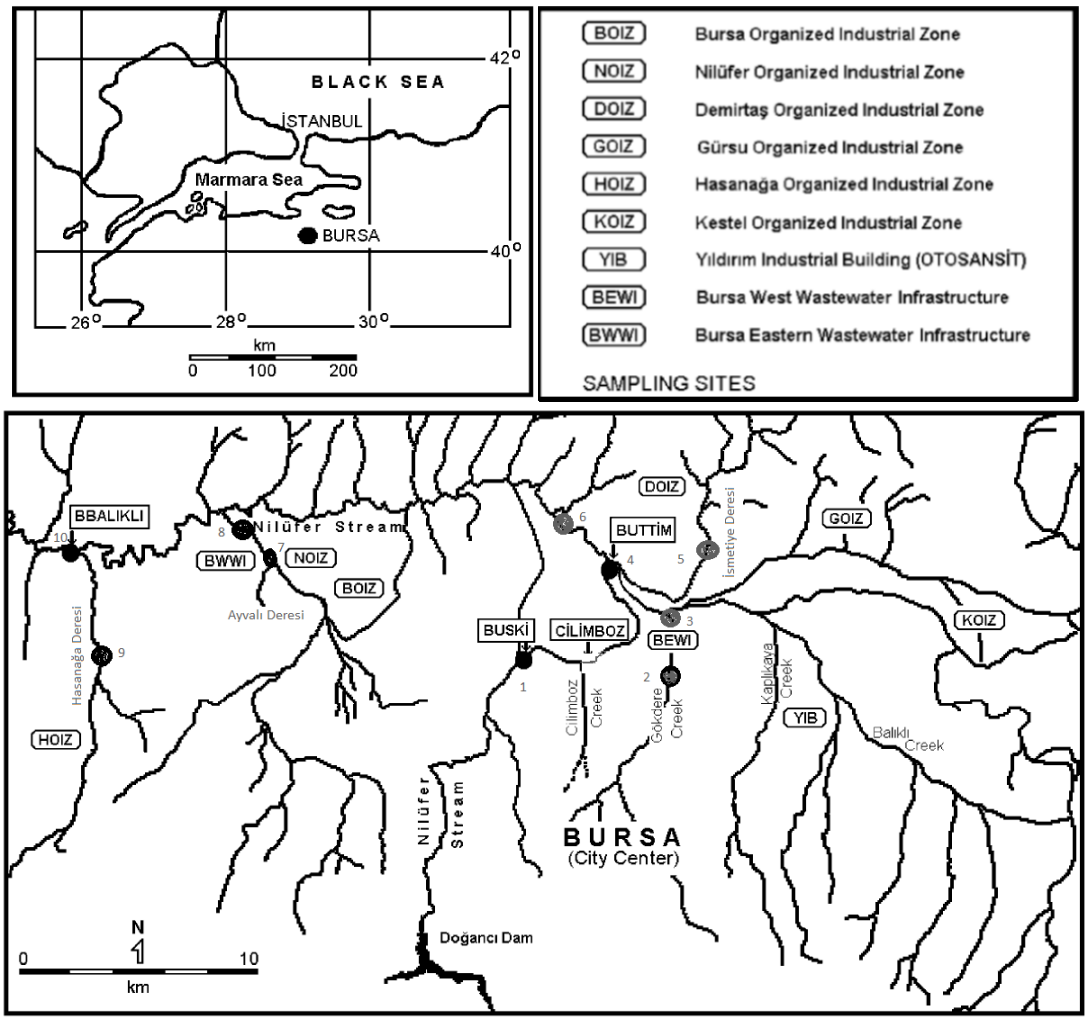

Figure 1. Location of Measuring Stations (Adapted from Güleryüz et al., 2008) [14].

2.3 Evaluation of the Health Risk of Arsenic

Arsenic enters into human body by the way of nutrition, dermal contact and inhalation [15]. The average daily dose (ADD) through potable water intake was estimated according to the following equation [16,17].

$$ADD = C \times IR \times ED \times EF / (BW \times AT) \quad (1)$$

In this equation ADD was the average daily dose during the exposure (mg/kg-day) and C represented the arsenic concentration in water (μg/L), IR was water consumption rate (2 liters for adults and one for children's), ED was duration of vulnerability (70 years for adults and 10 years for children), EF was exposure frequency (365 days' years 1), BW was body weight (72 kg for adults and 32.7 kg for children), and AT was average life time (25,550 days for adults and 3650 days for children) [17,18].

In this study, chronic and carcinogenic risk situation were evaluated. The HQ could be estimated by the following equation [16].

$$HQ = ADD / RfD \quad (2)$$

In this equation, RfD- the toxicity reference dose was 0.0003 mg/kg.day [19]. If the HQ values were >1 the human health risk was exist [17,18,20]. The equation of cancer risk (CR) was as below:

$$CR = ADD \times CSF \quad (3)$$

The cancer slope factor (CSF) of EPA for As is 1.5 mg/kg.day [19]. The CR value greater than one in million (10^{-6}) was generally considered significant by USEPA. All fixed coefficients and reference values from the literature in the calculations were used in μg/L.

3. Results and Discussion

3.1 Spatial Evaluation of Variation of Concentrations

To examine the temporal and spatial variation of arsenic, its concentrations between March 2015 and December 2021 were examined. Values between March 2015 and December 2019 were evaluated as pre-pandemic, and values between March 2020 and December 2021 were evaluated as post-pandemic.

When the values at the measurement stations before and after the COVID-19 pandemic were examined, it was seen that the concentrations at all stations increased, except for the 3rd Station. When the values before the pandemic were examined, it was seen that the highest concentration was 0.213 mg/L at the 10th Station and the lowest concentration was 0.0178 mg/L at the 1st Station. When the post-pandemic concentrations were examined, the highest concentration was again observed at the 10th Station (0.0358 mg/L), and the lowest concentrations were observed at the 3rd (0.0189 mg/L) and 1st and (0.0193 mg/L) Stations. The mean and standard deviation values of As concentrations before and after the pandemic at the measurement stations were given in Table 2.

Table 2. The Mean and standard deviations of pre-pandemic and post pandemic As concentrations

Stations	Pre-Pandemic		Post-Pandemic	
	Mean	Std	Mean	Std
1	0.0178	0.0068	0.0193	0.0053
2	0.0206	0.0056	0.0218	0.0049
3	0.0194	0.0067	0.0189	0.0048
4	0.0195	0.0056	0.0201	0.0047
5	Not Enough Measurements		Not Enough Measurements	
6	0.0192	0.0059	0.0206	0.0046
7	0.0208	0.0063	0.0318	0.0272
8	0.0200	0.0074	0.0358	0.0373
9	0.0196	0.0074	0.0223	0.0060
10	0.0213	0.0066	0.0358	0.0314

It was thought that the reason for the decrease in the concentrations at the 3rd station after the pandemic was the decrease in the pollution load coming to the Eastern Wastewater Treatment Plant because of the decrease in the production in the industry during the pandemic. The general and seasonal averages of all values before and after the pandemic were examined. Accordingly, when the 7-year general averages are examined, it was seen that the highest concentration was 0.0256 mg/L at the 8th Station, and the lowest concentration is 0.0182 mg/L at the 1st Station. When the 7-year spring, summer and winter averages were examined, it was observed that all the maximum values were 0.0221 mg/L, 0.0231 mg/L and 0.0337 mg/L at the 7th Station, respectively. The maximum autumn average was determined as 0.0309 mg/L at the 8th Station. The minimum values in the spring, autumn and winter seasons were determined as 0.0187 mg/L, 0.0181 mg/L and 0.0170 mg/L at Station 1, respectively. The 7-year general and seasonal averages at the measurement stations were given in Table 3.

The reason why the highest value according to the 7-year averages was at the 8th station was that the wastewater of Nilüfer and Bursa Organized Industrial Zones was discharged to the Western Wastewater Treatment Plant before this station. The 1st Station, where the minimum concentration was, located in the upstream part of the Nilüfer Stream. The fact that the maximum values were found at the 7th and 8th Stations as a result of the seasonal evaluations shown that these organized industrial zones contribute to the pollution.

When all the pre- and post-pandemic values were analyzed by years and stations, the highest values were measured as 0.0457 mg/L and 0.0675 mg/L at the 10th and 8th Stations in 2020 and 2021, respectively. The minimum value was found to be 0.0127 mg/L at the 9th Station in 2018. The variation graph of the concentrations by years and stations was shown in Figure 2.

EPA and WHO recommended permissible limits for arsenic in drinking water were 0.05 mg/L and 0.01 mg/L, respectively [17,18]. When all stations were examined for 7 years, it was determined that all the values were above the WHO standard, and the annual average of the 8th Station in 2021 was above the EPA standard and all other values were below EPA Standards. Potable water standard value of Turkey (TSE266) was the same as WHO, and none of the measurement stations were in compliance with the Turkish Drinking Water standard [21].

The arsenic limit value allowed in irrigation water was 0.10 mg/L according to the WHO's irrigation water usage guide [22]. Turkish irrigation water standard value was 0.05 mg/L [23]. According to these values, Nilüfer Stream was found to be suitable for irrigation water in terms of As parameter. Only in 2021, the general average of the 8th Station was higher than the Turkish Irrigation Standard.

3.2 Evaluation of Human Health Risk

When the water quality of Nilüfer Stream was evaluated in terms of human consumption risk, it was determined that the hazard quotient (HQ) values were greater than 1 at all stations before and after the pandemic, and therefore there was a chronic and carcinogenic risk. Before the pandemic, the order of magnitude in the stations in terms of HQ values was 10>7>2>8>9>4>3>6>1. The order of HQ magnitude in the stations of post-pandemic was 8>10>7>9>2>6>4>1>3. In general, post-pandemic HQ values and risk had generally increased. A decrease was observed only at the 3rd Station. According to the values before and after the pandemic, it was observed that the 8th and 10th stations had a higher risk, and the 3rd and 1st stations had a lower risk than the other stations.

Table 3. General and seasonal means of 7 Years in the measurement stations

Seasons	Stations									
	1	2	3	4	5	6	7	8	9	10
7 Years mean	0.0182	0.0217	0.0195	0.0202		0.0206	0.0239	0.0256	0.0203	0.0213
7 Years Spring mean	0.0187	0.0201	0.0203	0.0209		0.0203	0.0221	0.0196	0.0197	0.0212
7 Years Summer mean	0.0192	0.0229	0.0213	0.0216	Not Enough Value	0.0210	0.0231	0.0210	0.0203	0.0190
7 Years Autumn mean	0.0181	0.0227	0.0204	0.0204		0.0214	0.0234	0.0309	0.0223	0.0234
7 Years Winter mean	0.0170	0.0214	0.0190	0.0193		0.0201	0.0337	0.0327	0.0190	0.0192

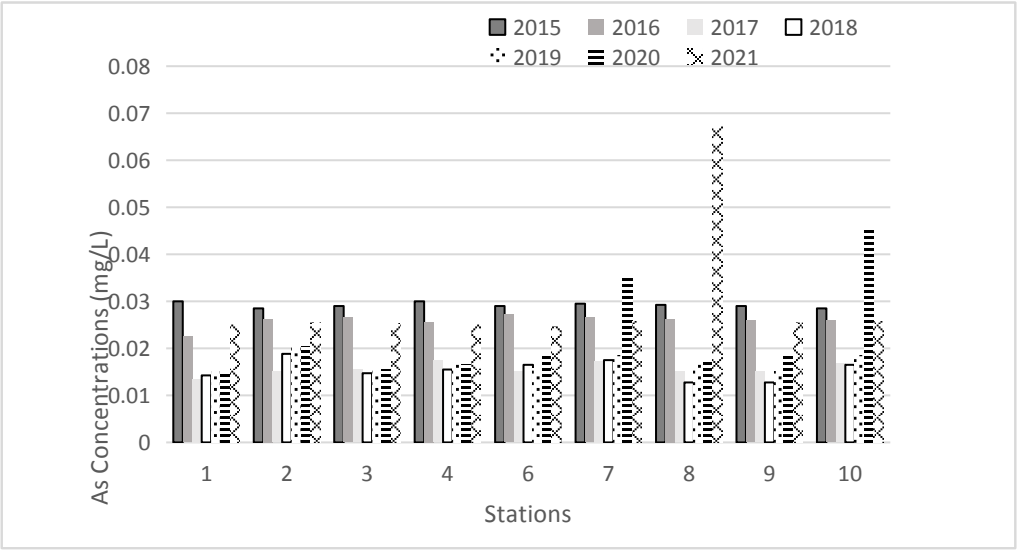

Figure 2. The variation graph of the concentrations by years and stations

The HQ order of the measuring stations was found as 8>7>2>10>6>9>4>3>1 according to the total 7-year averages before and after the pandemic. According to the post-pandemic and general average values, it could be said that the 8th Station had the highest risk, and the 3rd and 1st Stations had low risk.

When all HQ values were examined, it was seen that the highest value was 3.316 at Station 8 after the pandemic, and the lowest HQ value was at Station 1 before the pandemic with 1.615.

When the CR (carcinogenic risk) numbers were examined, it was hazardous for 7 years before and after the pandemic. After the pandemic, the values increased a little more. It was observed that the highest CR value was 14924×10^{-6} at the 8th Station after the pandemic, and the lowest was 743×10^{-6} at the 1st Station before the pandemic.

The 10th and 8th stations, where the concentrations were high, were located after the junction of the side streams and the discharge of Nilüfer and Bursa OIZs. Therefore, the pollution was more in there. The 1st Station was the upstream of the Stream, and the pollution sources were mixed later. Therefore, the health risk was found to be lower than the other stations. ADD, HQ and CR values calculated according to the general averages of 7 years before and after the pandemic were given in Table 4.

4. Conclusions

As a result of all the evaluations, it had been seen that Nilüfer Stream was not suitable for potable water quality according to National and International standards in terms of As parameter, but it was suitable for irrigation water quality.

After the pandemic, a decrease in pollution occurred, which was estimated to be due to the decrease in the production of the industrial zones located in the eastern part of the city only. However, pollution increased at all stations in other parts of the Stream. Therefore, the COVID-19 pandemic did not reduce As pollution. It had increased during the pandemic. It had been thought that the reason for this might be that the wastewater treatment plants did not carry out adequate treatment during the pandemic. Since the concentrations were higher than the standard values and a health risk in the upstream part where the point pollution sources were the least, it was shown that the pollution was not only caused by industry. It was also caused by the natural soil structure of the basin, mining activities and pesticide use. However, the increase in the concentration towards the downstream shown that the industry increased the pollution.

It was determined that the hazard quotient (HQ) values were greater than 1 at all stations before and after the pan-

Table 4. ADD, HQ and CR values calculated according to pre- and post-pandemic and 7-years general averages

Station	Pre-Pandemic			Post-Pandemic			Means of 7 years		
	ADD	HQ	CR	ADD	HQ	CR	ADD	HQ	CR
1	0.49537	1.6512	743×10^{-6}	0.535714	1.785714	804×10^{-6}	0.506667	1.688889	760×10^{-6}
2	0.57197	1.9066	858×10^{-6}	0.605556	2.018519	908×10^{-6}	0.603395	2.011317	905×10^{-6}
3	0.539352	1.7978	809×10^{-6}	0.524306	1.747685	786×10^{-6}	0.542088	1.806958	813×10^{-6}
4	0.540509	1.8017	811×10^{-6}	0.559524	1.865079	839×10^{-6}	0.559722	1.865741	840×10^{-6}
5	Not Enough Measurements								
6	0.534392	1.7813	802×10^{-6}	0.572222	1.907407	858×10^{-6}	0.571429	1.904762	857×10^{-6}
7	0.576389	1.9213	865×10^{-6}	0.883838	2.946128	13258×10^{-6}	0.663105	2.210351	995×10^{-6}
8	0.554167	1.8472	831×10^{-6}	0.994949	3.316498	14924×10^{-6}	0.710573	2.368578	1066×10^{-6}
9	0.543056	1.8102	815×10^{-6}	0.618056	2.060185	92710×10^{-6}	0.564484	1.881614	847×10^{-6}
10	0.590278	1.9676	885×10^{-6}	0.993056	3.310185	1489×10^{-6}	0.590278	1.967593	885×10^{-6}

demic, and therefore there was a chronic and carcinogenic risk. Post-pandemic HQ values and risk had generally increased.

As a result, in order to prevent As pollution, it must to examine in detail the industrial (point) and agricultural (diffuse) pollutant sources originating from pesticide usage and to take protective measures. It must carry out the necessary inspections especially regarding the mining activities in the basin.

Conflict of Interest

There is no conflict of interest.

References

[1] Mutlu, M., 2010. Arsenic Pollution and Health Risk Assessment in the Groundwater of Simav Plain, Kütahya. Master Thesis, Dokuz Eylül University Graduate School of Natural and Applied Sciences, İzmir.

[2] Henke, K., 2009. Environmental Chemistry, Health Threats and Waste Treatment. John Wiley & Sons Ltd. pp. 575, Chichester, UK.

[3] Başkan, B., Pala, M., 2009. Arsenic Contamination in Drinking Water: An Assessment for Turkey. Pamukkale University. Journal of Engineering Sciences. 15(1), 69-79.

[4] Garelick, H., Jones, H., Dybowska, A., et al., 2009. Arsenic pollution sources. Reviews of Environmental Contamination. 197, 17-60.
DOI: https://doi.org/10.1007/978-0-387-79284-2-2

[5] Erdol, S., Ceylan, S., 1997. Determination of arsenic contamination in water samples obtained from Bursa reqion. Journal of Uludag University Faculty of Veterinary. 16, 119-127.

[6] Gemici, Ü., Tarcan, G., Helvacı, C., et al., 2008., High arsenic and boron concentrations in groundwaters related to mining activity in the Bigadiç Borate Deposits (Western Turkey). Applied Geochemistry. 23, 2462-2476.
DOI: https://doi.org/10.1016/j.apgeochem.2008.01.013

[7] Karaer, F., Küçükballı, A., 2006. Monitoring of Water Quality and Assessment of Organic Pollution Load in the NiIlufer Stream, Turkey. Environmental Monitoring and Assessment. 114, 391-417.
DOI: https://doi.org/10.1007/s10661-006-5029-y

[8] Üstün, G.E., 2011. The Assessment of Heavy Metal Contamination in the Waters of the Nilüfer Stream in Bursa. Ekoloji. 20(81), 61-66.
DOI: https://doi.org/10.5053/ekoloji.2011.819

[9] Dorak, S., Çelik, H., 2020. Seasonal Variation of Some Trace Element and Heavy Metal Concentrations in a Turkish Stream. Polish Journal of Environmental Studies. 29(1), 589-600.
DOI: https://doi.org/10.15244/pjoes/101617

[10] Aydın, A.O., Gülensoy, H., Akıcıoğlu, A., et al., 2003. The Effect of Arsenic in Colemanites to Boric Acid and Borax Production. Journal of Balıkesir University Institute of Science and Technology. pp. 5-1.

[11] Smedley, P.L., Kinniburgh, D.G., 2002. A Review of the Source, Behaviour, and Distribution of Arsenic in Natural Waters. Applied Geochemistry. 17, 517-568.
DOI: https://doi.org/10.1016/S0883-2927(02)00018-5

[12] Bursa Province 2019 Environmental Report, 2019. Bursa Provincial Directorate of Environment and Urban Management. https://webdosya.csb.gov.tr/db/ced/icerikler/bursa_2019_cevre_durum_raporu-20201217210215.pdf (Access on 27 July 2022).

[13] Fianko, J.R., Osae, S., Adomako, D., et al., 2007. Assessment of Heavy Metal Pollution of the Iture Estuary in the Central Region of Ghana. Environmental Monitoring and Assessment. 131, 467-473,
DOI: https://doi.org/10.1007/s10661-006-9492-2

[14] Güleryüz, G., Arslan, H., Çelik, C., et al., 2008. Heavy Metal Content of Plant Species along Nilüfer Stream in Industrialized Bursa City, Turkey. Water, Air, and Soil Pollution. 195, 275-284.
DOI: https://doi.org/10.1007/s11270-008-9745-5

[15] Agency for Toxic Substances and Disease Registry, 2000. Toxicological Profile for Arsenic. US Department of Health and Human Services, Atlanta, Georgia.

[16] US Environmental Protection Agency (US EPA), 1998. Arsenic, Inorganic. United States Environmental Protection Agency, Integrated Risk Information System (IRIS), (CASRN 7440-38-2). http://www.epa.gov/iris/.

[17] Muhammad, S., Shah, M.T., Khan, S., 2010. Arsenic Health Risk Assessment in Drinking Water And Source Apportionment Using Multivariate Statistical Techniques in Kohistan Region, Northern Pakistan. Food and Chemical Toxicology. 48, 2855-2864.
DOI: https://doi.org/10.1016/j.fct.2010.07.018

[18] Radfard, M., Yunesian, M., Nabizadeh, R., et al., 2019. Drinking water quality and arsenic health risk assessment in Sistan and Baluchestan, Southeastern

Province, Iran. Human and ecological risk assessment: An International Journal. 25(4), 949-965.
DOI: https://doi.org/10.1080/10807039.2018.1458210

[19] US Environmental Protection Agency (US EPA), 2005. Guidelines for Carcinogen Risk Assessment. Risk Assessment Forum, Washington, DC, EPA/630/P-03/001F.

[20] Khan, S., Cao, Q., Zheng, Y.M., et al., 2008. Health risk of heavy metals in contaminated soils and food crops irrigated with wastewater in Beijing China. Environmental pollution. 152, 686-692.
DOI: https://doi.org/10.1016/j.envpol.2007.06.056

[21] TSE-266 (Turkish Standard), 2005. Regulation on water intended for human consumption, Turkish Standards, Ankara.

[22] Singh, R., Singh, S., Parihar, P., et al., 2015. Arsenic contamination, consequences, and remediation techniques: A review. Ecotoxicology and Environmental Safety. 112, 247-270.
DOI: https://doi.org/10.1016/j.ecoenv.2014.10.09

[23] Turkish Water Pollution Control Regulation, Regulation modified on Water Pollution Control Regulation, Official gazette No. 26786 (13 February 2008) (In Turkish).

BILINGUAL PUBLISHING CO.
Pioneer of Global Academics Since 1984

Journal of Metallic Material Research
https://ojs.bilpublishing.com/index.php/jmmr

ARTICLE

Producing High Purity Nickel Metal Powder from Nickel Wastes through Acidic Leaching by Sulfuric Acid

Mohammad Bagher Oshrieh Khanali Nekouee* Hasan Abbaszadeh

Faculty of Materials and Manufacturing Technologies, Malek Ashtar University of Technology, Iran

ARTICLE INFO

Article history
Received: 8 July 2022
Revised: 27 July 2022
Accepted: 29 July 2022
Published Online: 22 August 2022

Keywords:
Nickel
Metal powder
Recovery
Acidic leaching
Sulfuric acid

ABSTRACT

Nickel has found increasing application in electronic, automobile manufacturing, plating, and metal industries and so on. Producing high quality metal powders to satisfy increasing demand for advanced materials is of very high importance. There are a few numbers of standard powder production techniques. An acidic leaching has been applied in present research. Sulfuric acid has been used to leach nickel wastes of plating industry. To produce nickel oxide powder furnaces with no protecting atmosphere and to produce pure nickel powder, tube furnace with hydrogen atmosphere has been applied. Variables performed in the research are time, density of sulfuric acid, and amount of hydrogen peroxide. To analyze powders produced, EDS element analysis and to determine size of powder particles, SEM has been applied. It was shown by the results that the highest amount of nickel dissolution in sulfuric acid (98%) has taken place during one hour and there is a direct relationship between hydrogen peroxide amount and nickel dissolution in sulfuric acid.

1. Introduction

Nickel as 24th metal element is one of the most frequent element available in earth's crust. Wide range usage made of nickel in different industries has led it to be considered as a strategic metal. In fact, this variety of application is resulted from various physical and chemical properties of this metal [1,2]. This is one of the important metals in industry and a basic one for modern technologies and industry. It is also important in energy, telecommunication, shape memory alloy, and electronics industries that are necessary for economy, medical industry and or substructures [3,4]. Some studies have been performed in this respect which will be referred to.

Mansi et al. [5] with leaching of catalysts in a solution of 50% sulfuric acid, solid to liquid ratio 1:12 and in particle size less than 500 microns for 5 hours, at 100 °C with a stirring of 800 rpm, about 99% Recover of nickel. Oza et al. [6] used ultrasound to recover nickel from the catalysts along with the leaching method. In this work, they were able to extract about 95% of nickel from the text of nickel-alumina catalysts by nitric acid at a concentration

*Corresponding Author:
Khanali Nekouee,
Faculty of Materials and Manufacturing Technologies, Malek Ashtar University of Technology, Iran;
Email: khnekuee@gmail.com

DOI: https://doi.org/10.30564/jmmr.v5i2.4877
Copyright © 2022 by the author(s). Published by Bilingual Publishing Co. This is an open access article under the Creative Commons Attribution-NonCommercial 4.0 International (CC BY-NC 4.0) License. (https://creativecommons.org/licenses/by-nc/4.0/).

of 40% at 90 °C and a solid to liquid ratio of 1:10 (g/mL) for 50 minutes. Using ultrasound, the recovery time was reduced from 7 hours to 50 minutes.

Randhawa et al. [7] conducted a study in which the leaching kinetics of nickel-cadmium batteries by sulfuric acid were investigated. Their results showed that the concentration of sulfuric acid up to 10% had a significant effect on the recovery of cadmium and nickel. However, nickel recovery was much lower than cadmium. Addition of hydrogen peroxide improved the nickel leaching kinetics, and nickel recovery increased to 96% at 5 hours of leaching, and nickel leaching also increased with increasing temperature. Driss et al. [8] used sulfuric acid and hydrochloric acid to recover nickel from palm oil catalysts. In this work, they investigated the effect of acid concentration parameters, solid to liquid ratio, temperature and leach time and found that sulfuric acid is more effective for nickel recovery. If the concentration of sulfuric acid is 67%, the leaching time is 140 minutes, the solid to liquid ratio is 1:14, about 60% of nickel will be recovered at 60 °C. If the temperature is above 80 degrees Celsius, this value will decrease.

In another study by Abrar et al. [9], the recovery of nickel from a catalyst was investigated using the pressure dissolution method in nitric acid. The catalyst for this study is NiO/Al_2O_3, which is used for direct reduction and production of sponge iron. Results showed that at 140 °C maximum dissolution can be obtained but over this optimum temperature a reverse effect is noticed. Another important factor is the Rpm change effect, as a change from 600 to 300 caused a decrease of 10% of dissolution efficiency. Finally, it is shown that efficiency was improved when dissolution time increased.

Gharabaghi et al. [10] conducted a study entitled leaching kinetics of nickel extraction from hazardous scrap by sulfuric acid and optimization of dissolution conditions. It was found that nickel extraction increases with increasing sulfuric acid concentration, temperature and leaching time. Reducing particle size and solid to liquid ratio increased the dissolution of nickel. The extraction speed increased with increasing stirring speed and reached the highest level at 500 rpm. The maximum leaching rate was 97% at 25 °C after 30 minutes.

Liu and et al. [11] conducted research to produce high-purity basic nickel carbonate through chemical precipitation. They used electric double layer model to illustrate the adsorption mechanism of ions of sodium and chlorine and other impurities on solid surface. Experimental results indicate that the new process is very effective to remove Na^+ and Cl^- to a level of both less than 0.01 wt%. Li and et al. [12] also conducted research for the hydrothermal synthesis of nickel or cobalt-based carbonate hydroxides used in the production of supercapacitor electrodes. The results showed that the nickel-cobalt carbonate hydroxide electrode shows excellent cycling stability and is suitable for the production of supercapacitors.

In a study, Wu and et al. [13] produced nickel nanoparticles used in supercapacitors using hydrazine hydrate reduction. After conducting the experiment, nickel nanoparticles with a particle size of about 12 nm were obtained and they concluded that due to the good conductivity of nickel particles, it is a suitable option for producing supercapacitors. Huang and et al. [14] investigated the method by which nickel nanoparticles were produced. In this method, the production cost was reduced and nickel nanoparticles in the range of 180 nm to 260 nm were produced. They also controlled the size range of nickel particles by adjusting the reaction molar ratio and concentration. In one study, Li and et al. [15] produced ultrafine nickel powder and crystalline film using chemically controlled reduction. Their results showed that pure black nickel powder can be obtained when the pH > 10.0 and the temperature is in the range of 85 °C ~ 958 °C. RF plasma synthesis of nickel nanopowders via hydrogen hydroxide/nickel carbonate reduction was performed by Bai et al. [16]. They were able to produce nickel nanoparticles in the size range of 60 nm to 100 nm, which are used in the production of electrode materials.

Ultra fine nickel powder was produced by polyol method and its oxidation product by Zhou and et al. [17]. The results of this research showed that the high content of water in $Ni(OH)_2$ increases the reaction rate in the solution and decreases the average particle size of nickel powders. Paserin and et al. [18] investigated different methods for the mass production of nickel-based nanomaterials by the carbonyl process in a review article. In the research conducted by Alena and et al. [19], the structure and properties of nickel nanoparticles prepared by selective leaching were investigated. They came to the conclusion that with this method it is possible to achieve a particle size of less than 5 nm and by increasing the temperature from 20 °C to 80 °C, the particle size will be in the range of 10 nm to 15 nm. Archana and et al. [20] conducted a research titled recovery of nickel powder from copper electrolyte by electrolysis. They were able to recover 87% of the nickel, which increased to 99% under certain conditions. The purity of the produced powder was 89.99%.

Since nickel powder is one of the basic and important metals in the industry, the production of this powder with high purity will be of special importance. After a lot of

research, we came to the conclusion that one of the important sources for the production of nickel powder is the use of nickel wastes, especially nickel wastes produced by electroplating. As shown in the research, one of the best methods for producing metal powder is the acid leaching method. For this reason, we decided to produce high-purity nickel powder, which is used in various industries, from nickel waste by acid leaching method, which will be fully explained in the following process.

2. Materials and Method

Main materials used in the research have been prepared from plating wastes. EDS analysis of the material is shown in Figure 1. For acidic leaching of the material also, sulfuric acid Merck (98 wt%) has been used.

Reaction times have been selected 5, 10, 20, 30, 40, 50, and 60 minutes; while, sulfuric acid concentrations have been 20%, 40%, 60%, 80%, and 98%. One of the methods to increase dissolution speed of nickel wastes in sulfuric acid is adding H_2O_2 which effect of it has been studied through adding 50 cc, 100 cc, 150 cc, 200 cc, and 250 cc of the material. To stir and heat the solution in different stages of producing nickel powder, IKA/RCT basic hot plate stirrer (made in Germany) has been used. Producing nickel carbonate from nickel sulfate would be performed by sodium carbonate. Industrial type of sodium carbonate has been used in present research. To better perform the reaction between nickel sulfate and sodium carbonate, the temperature of the hot plate was set to 60 degrees Celsius. After finishing the reaction (Chemical reaction 2) and producing nickel carbonate, filter paper (Whatman) was used to separate the solution from it. There is a possibility that there is sodium in the nickel carbonate, which requires a lot of washing to remove it, because sodium is soluble in water. To do so, distilled water has been used to produce nickel oxide and finally pure nickel, two different furnaces with controlling atmosphere have been required. In the research and to produce nickel oxide from nickel carbonate; ordinary furnace (AZAR-FURNACE M35L) with no controlling atmosphere has been used for one hour at 700 °C (Chemical reaction 3). Finally, a hydrogen Fulled tube furnace (AZAR-FURNACE TF5/25) was used to convert nickel oxide into high purity nickel powder (Chemical reaction 4). The reduction process took place in two different cycles. The first cycle was performed at 700 °C for 2 hours and the second cycle at 600 °C for 4 hours. In general, production stages of nickel powder from nickel wastes include the four following stages:

Producing nickel sulfate from nickel wastes:
$(H_2SO_4 + Ni = NiSO_4 + H_2)$ (1)

Producing nickel carbonate from nickel sulfate:
$(NiSO_4 + Na_2CO_3 = NiCO_3 + Na_2SO_4)$ (2)

Producing nickel oxide from nickel carbonate:
$(NiCO_3 = NiO + CO_2)$ (3)

Producing high purity nickel powders from nickel oxide:
$(NiO + H_2 = Ni + H_2O)$ (4)

General production procedure of nickel powder is shown in Figure 2.

To determine EDS point analysis and to image produced powders, Vega/TScan SEM (made in China) has been used. Minimum diameter of the device where the sample is contacted is 2 nanometers.

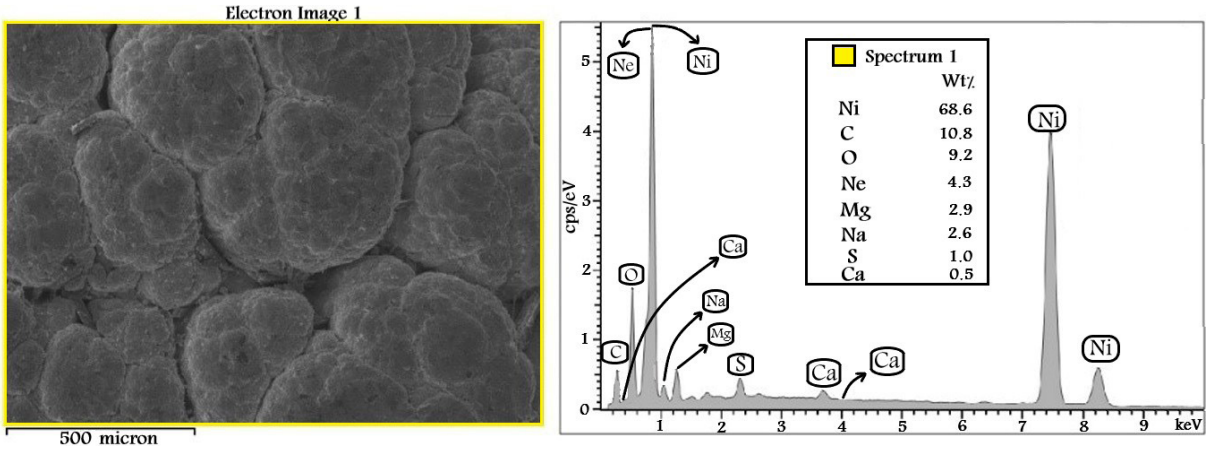

Figure 1. EDS analysis of wastes used in the research.

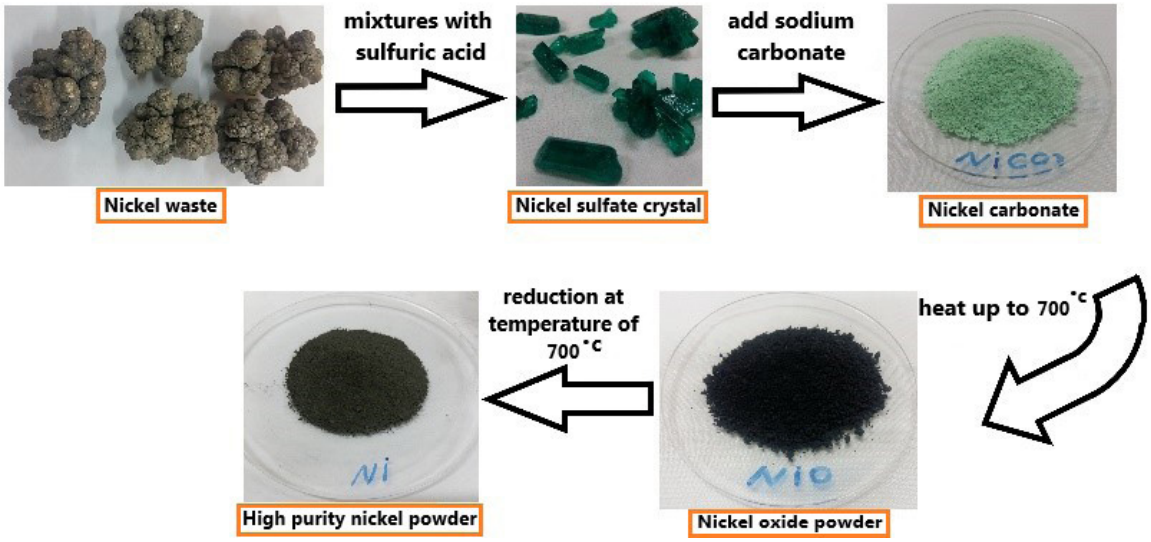

Figure 2. Flowchart of the research to produce high purity nickel powder.

3. Results and Discussion

After all four stages of producing nickel powder through acidic leaching, amounts of the product obtained in tests with final product have been computed and compared in reactions. In Table 1, the obtained have been compared with reaction stoichiometry reactions. At first stage, final product is nickel sulfate.

According to stoichiometry of the reaction, about 59.84 gr nickel would be dissolved in 100 gr sulfuric acid. The test and solving nickel waste in sulfuric acid has been performed for several times; and, nickel amount dissolved has been about 15 gr ~ 20 gr. End of the test has been considered to be at the point that no additional nickel would be dissolved in the solution and it would be considered as saturated. Final product of the second stage is nickel carbonate. According to the reaction stoichiometry, 68.48 gr sodium carbonate has to be consumed in each 100 gr of nickel sulfate so that the reaction would be complete; and, finally, there would be 76.7 gr nickel carbonate. This amount of sodium carbonate used for produced nickel sulfate in the research is very high; because, less nickel has been dissolved in sulfuric acid, compared to stoichiometry. Therefore, different amounts of sodium carbonate have been tested. Finally, it became clear that 30 gr sodium carbonate is appropriate for each 100 gr of nickel sulfate solution and the reaction would be complete. Third and fourth stages are well matched with stoichiometry. High difference in stages one and two can be due to type of nickel wastes used as well as purity of acid. Numbers obtained in stoichiometries reactions' will consider all conditions as ideal which their performance would be very hard and sometimes impossible in practical and lab conditions.

As referred to in the Research Materials and Method, one of the most important parameters in increasing dissolution of nickel wastes is sulfuric acid concentration, time and amount of hydrogen peroxide. The results obtained

Table 1. Comparing reaction products obtained in the research through stoichiometry.

Stage number	Final product	Final weight of the product in the laboratory	Final product weight according to stoichiometry	Difference (%)
1	$NiSO_4$	52.73	157.78	66.5
2	$NiCO_3$	33.6	76.7	56.2
3	NiO	61.36	62.92	2.46
4	Ni	77.17	78.57	1.27

from effect of these three parameters in dissolution of nickel wastes in sulfuric acid would be presented in this paper. Figure 3 shows effect of sulfuric acid concentration on amount of nickel wastes' dissolution. The test for all concentrations has been performed during one hour. As shown in the above figure, through increase of sulfuric acid concentration, dissolution amount of nickel wastes would be increased. At 20% and 40% concentrations, dissolution amount is very low and there is no main difference between the two concentrations; however, at 60% to 98% concentrations, a steep slope would be created in dissolution of nickel wastes. This shows that sulfuric acid with concentrations more than 60% can end to acceptable results.

In continuation of studying parameters, effect of reaction time duration has been dealt with. The test has been performed in sulfuric acid (98%), showing the highest efficiency in terms of dissolution in previous section. The results are provided in Figure 4. Figure 4 showed that, through increase of dissolution process time, more nickel wastes have been dissolved in sulfuric acid. This dissolution would be continued till saturation of the solution.

Another important parameter studied was the effect of amount of hydrogen peroxide on amount of dissolution (Figure 5). The test has been performed during one hour dissolution time in sulfuric acid (98%).

It became clear that adding hydrogen peroxide has a positive effect in increasing dissolution of nickel wastes in sulfuric acid. The reason for increased dissolution is increased oxidation and activation of surface of nickel wastes. As shown by the results, in previous test and during one hour 15.3 gr nickel wastes have been dissolved in sulfuric acid (98%). This amount has been increased to 16.91 gr after adding 50 cc hydrogen peroxide to the solution, through increasing of hydrogen peroxide to the solution, dissolution amount of nickel wastes also has been increased. To study purity of nickel powder produced in the research, EDS element analysis has been performed on powders (Figure 6).

Nickel powder produced is of 99.6% purity which is high; however, existence of 0.4% of sulfur in analyses of powders can be due to following reasons: firstly, in initial analysis of nickel wastes there is about 1% sulfur which has been remained till the final stage of powder production. Secondly, the reason justifying this amount of sulfur goes back to the first stage of nickel powder production and preparation of nickel sulfate through sulfuric acid. To study shape of nickel powder particles produced, images from SEM are shown in Figure 7.

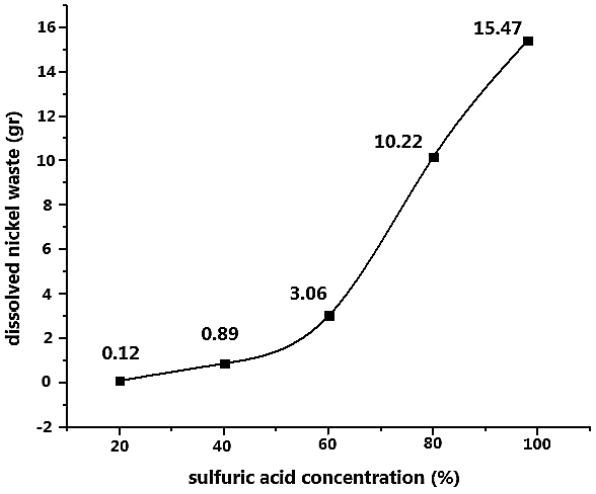

Figure 3. Effect of sulfuric acid concentration in dissolution of nickel wastes.

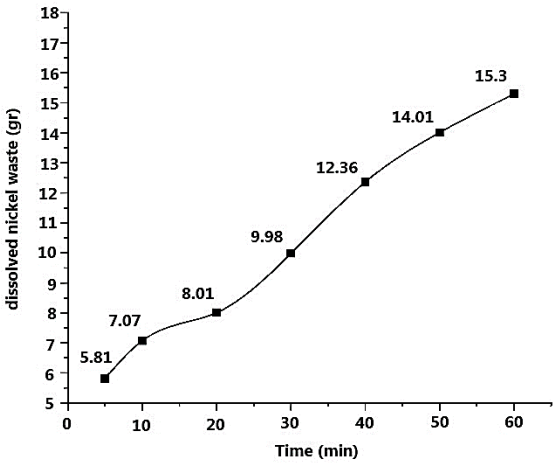

Figure 4. Effect of reaction time duration on dissolution of nickel wastes.

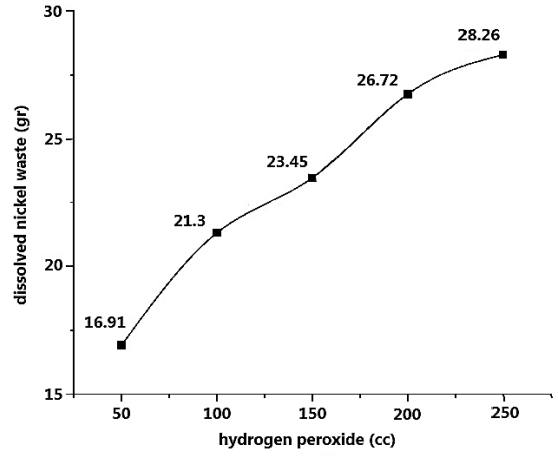

Figure 5. Effect of amount of hydrogen peroxide on dissolution of nickel wastes.

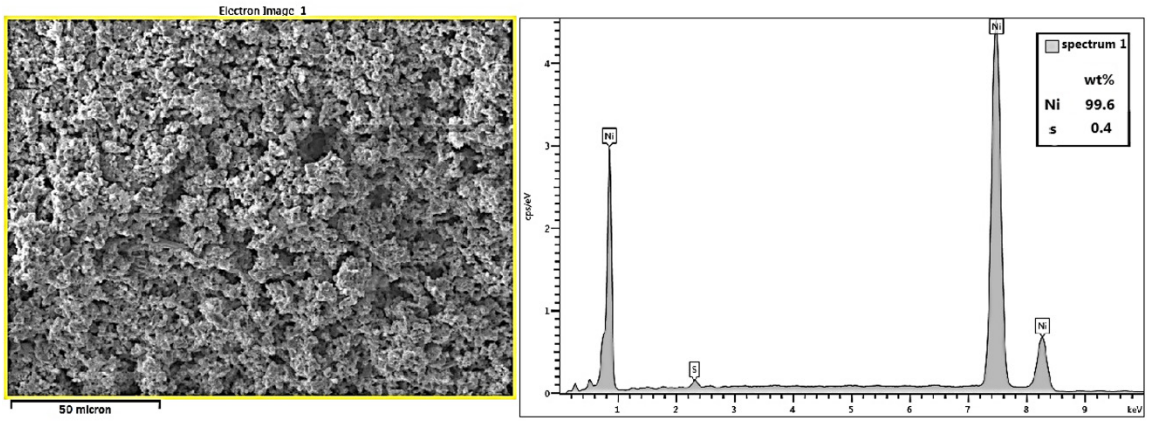

Figure 6. EDS element analysis performed on produced nickel powder.

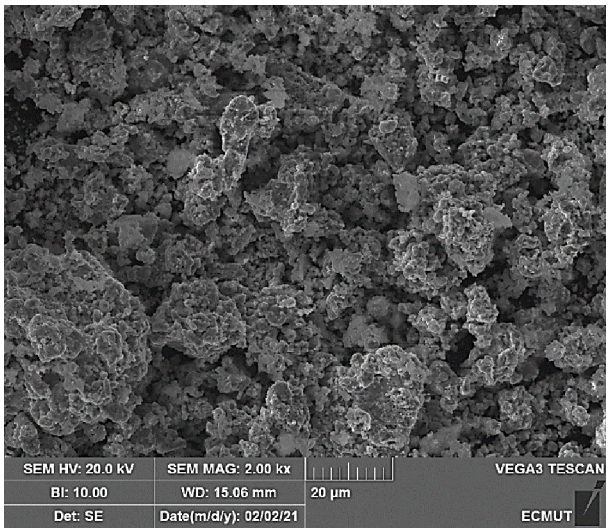

Figure 7. SEM images from nickel powder produced.

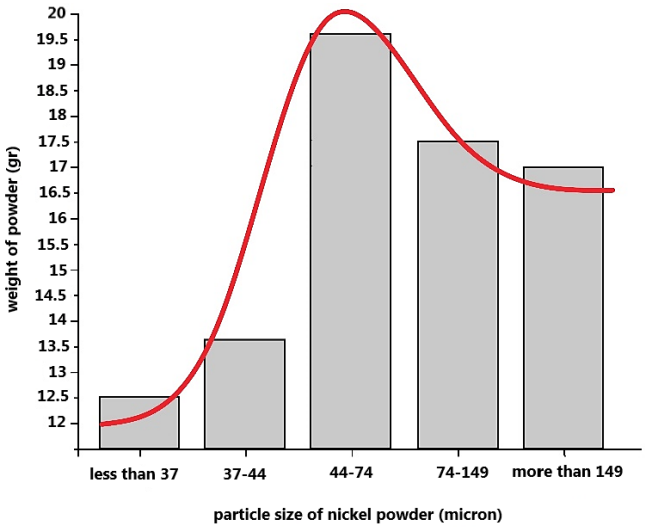

Figure 8. Size distribution of nickel powder produced in the research.

It can be suggested that powder particles produced had porous and irregular shape. To determine size distribution of produced powder particles, sifting is one of the common methods. To do so, 80 gr of nickel powder has been separated and passed through screen to determine size of particles. Size distribution of powder particles is shown in Figure 8.

The highest distribution is related to the range of 44 microns ~ 74 microns. Size of powder particles during third and fourth stages related to production of nickel oxide and pure nickel can be controlled. If at reduction stage of powders, temperature would be reduced and time would be increased; lower size of particles would be resulted. Therefore, the reduction temperature was 600 °C and the time was 4 hours. Elemental analysis (EDS) of nickel powder produced was performed after the completion of this cycle (Figure 9). As shown in the Figure 9, the nickel analysis shows a value of 100%.

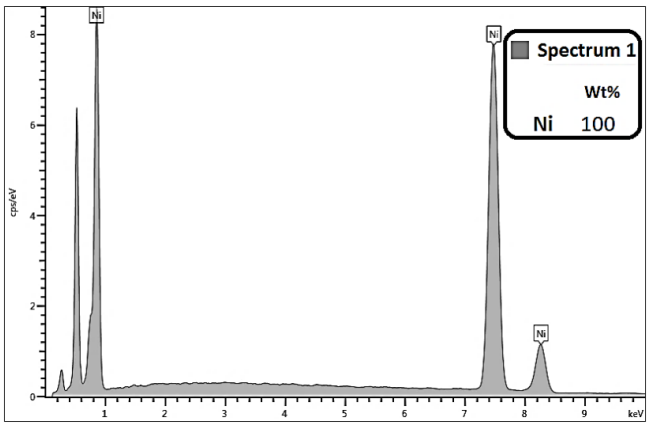

Figure 9. Elemental analysis (EDS) of nickel powder after a cycle of 600 °C and a time of 4 hours.

SEM images were also obtained from samples of powders produced in this cycle (Figure 10). Due to this shape and compared to the sample of powders produced from the previous cycle and Figure 7, the produced powders were much finer. The dispersion of the powder particle size produced in the second cycle was measured (Figure 11). According to this figure, 80.22% of the produced powders were less than 45 microns.

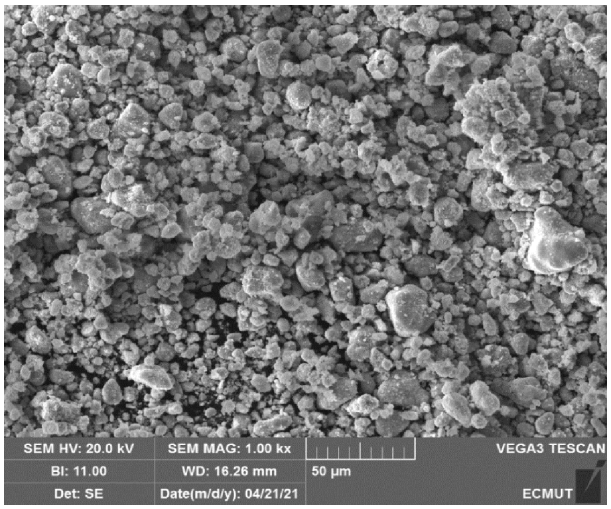

Figure 10. SEM image of nickel powder produced after the second reduction cycle.

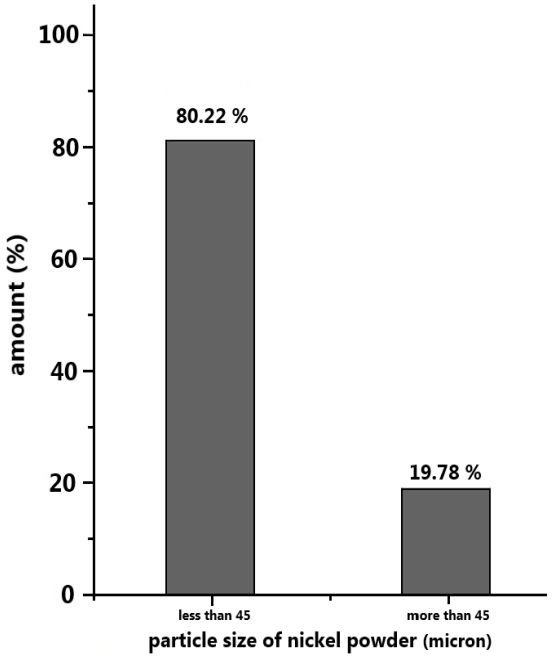

Figure 11. Nickel powder particle size dispersion after the second reduction cycle.

4. Conclusions

Acidic leaching to produce high purity nickel powder from nickel wastes through sulfuric acid has been performed in the research and the results are as follows:

1) The two parameters of sulfuric acid concentration and duration of process have had a direct effect on dissolution of nickel wastes in sulfuric acid. That is, upon increase of acid concentration from 20% to 98%, dissolution amount of nickel wastes has been increased from 0.12 gr to 15.47 gr. Also, upon increasing of time from five to 60 minutes, dissolution amount of nickel wastes has been increased from 0.81 gr to 15.3 gr.

2) Hydrogen peroxide (H_2O_2) has been considered as one of the main and important factors in increasing dissolution of nickel wastes in sulfuric acid. That is during one hour fixed, 15.3 gr ~ 15.47 gr of nickel wastes have been dissolved in the solution with no hydrogen peroxide; however, adding 50cc of hydrogen peroxide during the same time has led to increase of nickel wastes' dissolution to about 16.91 gr. This is about 10% higher than the time no hydrogen peroxide has been used. In industrial scale, it is considered as a considerable amount. In general and upon increase of hydrogen peroxide, dissolution amount of nickel wastes also has been increased due to surface of nickel wastes becoming activated.

3) Nickel powder produced through acidic leaching has been highly pure. Elemental analysis (EDS) of this powder in the first reduction cycle (temperature 700 °C and time 2 hours), showed 99.6%, which is considered as an acceptable purity. Also, particles of nickel powder have been porous and irregular. Size range of nickel powder has been computed and maximum value has been related to size of particles within the range of 44 microns ~ 74 microns.

4) After the second reduction cycle (temperature of 600 °C and time of 4 hours), elemental analysis of the produced nickel powder showed 100%. Also, after this cycle, the particle size of nickel powder became smaller than the first cycle. Most of the particle size dispersions were obtained in the range below 45 microns.

Conflict of Interest

There is no conflict of interest.

References

[1] Rhamdhani, M.A., Jak, E., Hayes, P.C., 2008. Basic nickel carbonate: Part I. Microstructure and phase changes during oxidation and reduction processes. Metallurgical and Materials Transactions B. 39(2), 218-233.
DOI: https://doi.org/10.1007/s11663-007-9124-4

[2] Rhamdhani, M.A., Jak, E., Hayes, P.C., 2008. Basic

nickel carbonate: Part II. Microstructure evolution during industrial nickel production from basic nickel carbonate. Metallurgical and Materials Transactions B. 39(2), 234-245.
DOI: https://doi.org/10.1007/s11663-008-9139-5

[3] Mackenzie, M., Virnig, M., Feather, A., 2006. The recovery of nickel from high-pressure acid leach solutions using mixed hydroxide product–LIX® 84-INS technology. Minerals Engineering. 19(1), 1220-1233.
DOI: https://doi.org/10.1016/j.mineng.2006.01.003

[4] Shaheen, W.M., 2002. Thermal behaviour of pure and binary basic nickel carbonate and ammonium molybdate systems. Materials Letters. 52(4-5), 272-282.
DOI: https://doi.org/10.1016/S0167-577X(01)00406-2

[5] Al-Mansi, N.M., Abdel Monem, N.M., 2002. Recovery of nickel oxide from spent catalyst. Waste Management. 22(1), 85-90.
DOI: https://doi.org/10.1016/S0956-053X(01)00024-1

[6] Oza, R., Nikhil, S., Sanjay, P., 2011. Recovery of nickel from spent catalysts using ultrasonication-assisted leaching. Journal of Chemical Technology & Biotechnology. 86(10), 1276-1281.
DOI: https://doi.org/10.1002/jctb.2649

[7] Randhawa, N.S., Kalpataru, G., Manoj, K., 2016. Leaching kinetics of spent nickel–cadmium battery in sulphuric acid. Hydrometallurgy. 165(1), 191-198.
DOI: https://doi.org/10.1016/j.hydromet.2015.09.011

[8] Idris, J., Musa, M., Yin, C.Y., et al., 2010. Recovery of nickel from spent catalyst from palm oil hydrogenation process using acidic solutions. Journal of Industrial and Engineering Chemistry. 16(2), 251-255.
DOI: https://doi.org/10.1016/j.jiec.2010.01.044

[9] Abrar, B., Mohammad, H., Ali, P., 2016. Recovery of nickel from reformer catalysts of direct reduction, using the pressurized dissolving method in nitric acid. Engineering, Technology & Applied Science Research. 6(5), 1158-1161.
DOI: https://doi.org/10.48084/etasr.731

[10] Gharabaghi, M., Mehdi, I., Amir, R.A., 2013. Leaching kinetics of nickel extraction from hazardous waste by sulphuric acid and optimization dissolution conditions. Chemical Engineering Research and Design. 91(2), 325-331.
DOI: https://doi.org/10.1016/j.cherd.2012.11.016

[11] Liu, F., Li, N., Zhang, Z., et al., 2008. An improved purification method for preparation of basic nickel carbonate of high purity via chemical precipitation. Journal of Wuhan University of Technology-Mater. 23(3), 331-333.
DOI: https://doi.org/10.1007/s11595-007-3331-3

[12] Li, Y., Li, P., Xin, Z., 2017. Hydrothermal synthesis of hierarchical nickel-or cobalt-based carbonate hydroxides for supercapacitor electrodes. International Journal of Electrochemical Science. 12, 4016-4024.
DOI: https://doi.org/10.20964/2017.05.50

[13] Wu, X., Xing, W., Zhang, L., 2012. Nickel nanoparticles prepared by hydrazine hydrate reduction and their application in supercapacitor. Powder Technology. 224, 162-167.
DOI: https://doi.org/10.1016/j.powtec.2012.02.048

[14] Huang, G.Y., Xu, S.M., Gang, X.U., et al., 2009. Preparation of fine nickel powders via reduction of nickel hydrazine complex precursors. Transactions of Nonferrous Metals Society of China. 19(2), 389-393.
DOI: https://doi.org/10.1016/S1003-6326(08)60283-6

[15] Li, Y.D., Li, C.W., Wang, H.R., et al., 1999. Preparation of nickel ultrafine powder and crystalline film by chemical control reduction. Materials Chemistry and Physics. 59(1), 88-90.
DOI: https://doi.org/S0254-0584(99)00015-2

[16] Bai, L., Fan, J., Hu, P., et al., 2009. RF plasma synthesis of nickel nanopowders via hydrogen reduction of nickel hydroxide/carbonate. Journal of Alloys and Compounds. 481(1-2), 563-567.
DOI: https://doi.org/10.1016/j.jallcom.2009.03.054

[17] Ying, Z., Shengming, J., Guanzhou, Q., et al., 2005. Preparation of ultrafine nickel powder by polyol method and its oxidation product. Materials Science and Engineering: B. 122(3), 222-225.
DOI: https://doi.org/10.1016/j.mseb.2005.06.006

[18] Paserin, V., Baksa, S., Zaitsev, A., et al., 2008. Potential for mass production of nickel-based nanomaterials by carbonyl process. Journal of Nanoscience and Nanotechnology. 8(8), 4049-4055.
DOI: https://doi.org/10.1166/jnn.2008.AN44

[19] Michalcová, A., Svobodová, P., Nováková, R., et al., 2014. Structure and magnetic properties of nickel nanoparticles prepared by selective leaching. Materials Letters. 137, 221-224.
DOI: https://doi.org/10.1016/j.matlet.2014.09.012

[20] Agrawal, A., Bagchi, D., Kumari, S., et al., 2007. Recovery of nickel powder from copper bleed electrolyte of an Indian copper smelter by electrolysis. Powder Technology. 177(3), 133-139.
DOI: https://doi.org/10.1016/j.powtec.2007.03.032

BILINGUAL PUBLISHING CO.
Pioneer of Global Academics Since 1984

Journal of Metallic Material Research
https://ojs.bilpublishing.com/index.php/jmmr

REVIEW

Anti-bacterial Properties of Transition Metal Complexes of Copper Metal Ion: A Mini Review

Abhay Nanda Srivastva[1,2*] Nisha Saxena[3] Netra Pal Singh[4] Jayant Kumar[5]

1. Department of Chemistry, Nitishwar Mahavidyalaya, B. R. A. Bihar University, Muzarrafpur, 842002, India
2. University Department of Chemistry, B. R. A. Bihar University, Muzaffarpur, 842001, India
3. Department of Chemistry, M. R. M. College, L. N. Mithila University, Darbhanga, 846004, India
4. Department of Chemistry, D. D. U. Gorakhpur University, Gorakhpur, 273009, India
5. Graduate Student, Department of Zoology, Nitishwar Mahavidyalaya, B. R. A. Bihar University, Muzarrafpur, 842002, India

ARTICLE INFO

Article history
Received: 27 June 2022
Revised: 03 November 2022
Accepted: 04 November 2022
Published Online: 17 November 2022

Keywords:
Ligands
Coordination compounds
Antimicrobial activity
Drug resistance

ABSTRACT

Bacterial infections are a major cause for impulsive deaths in human beings. Bacterial infections of the respiratory, gastrointestinal and central nervous system account for the majority of cases of sudden casualties. Readily available drugs are getting ineffective by each passing day as the mutation is very fast in these pathogenic microbes resulting in drug resistance. The growing resistance of bacteria necessitates the development of new and effective compounds of desired characteristics that could bar the rapid development of bacterial cell inside of the host body. Along with cellular resistance for clinical antibiotics, co-bacterial infections during microbial attacks (*viz.* virus, fungus, protozoans etc.) also demand for some novel antibacterial drugs having high efficacy and minimal side effects on human body. These antibiotics should also be compatible with remedies ongoing for core microbial infections. So, in demand of search for effective antibacterial moieties, the scope of transition metal complexes as drug gives a good signal against the pathogenic bacteria by inhibiting their growth. The action of metal complexes on bacterial cell may be due to impremiablity, enzymatic interruptions, ribosomal interactions, disturbance in the path of protein synthesis, denaturing of genetic materials etc. inside the cell. Metals in complexes may interrupt the lipophilisity through the bacterial cell wall. Inclusion of metal ions in organic moieties behaving as ligand delocalize π-electrons upon the entire chelate ring and this chelation results in overlapping of ligand orbital and partial sharing of (+)ve charge of metal ion with donor atoms. These structural modifications in metal and organic lone pair donor species are the supposed reasons for their enhanced antimicrobial activities against pathogenic microbes. The present review focuses on the impact of recently synthesized, well characterized mono and binuclear transition metal complexes of Cu ions that have the potential to be the drug of the decade in medicinal inorganic chemistry for treating the bacterial diseases.

*Corresponding Author:
Abhay Nanda Srivastva,
Department of Chemistry, Nitishwar Mahavidyalaya, B. R. A. Bihar University, Muzarrafpur, 842002, India; University Department of Chemistry, B. R. A. Bihar University, Muzaffarpur, 842001, India;
Email: abhay_s1986@yahoo.co.in

DOI: https://doi.org/10.30564/jmmr.v5i2.4836
Copyright © 2022 by the author(s). Published by Bilingual Publishing Co. This is an open access article under the Creative Commons Attribution-NonCommercial 4.0 International (CC BY-NC 4.0) License. (https://creativecommons.org/licenses/by-nc/4.0/).

1. Introduction

Discovery of *cis*-platin opened the door for the exploration of an enormous number of other biologically active metal complexes [1,2]. It was then a new interest of the pioneer to synthesize novel transition metal complexes. Transition metals complexes with metal ion/s and a variety of ligands developed from organic and/ or inorganic moieties were of interest of chemists for the structural elucidation and their applications in various emerging field of science and technology [3,4]. Transition metal complexes have shown their importance in all the area of chemistry serving to society [5-7]. Among different applications, metal complexes are studied as potent drug molecules against many day to day life diseases to lethal diseases, *viz.* general microbial infections, diabetes, inflammation, cancer, acquired immune deficiency syndrome, Alzheimer, Parkinson etc. Among various therapeutic potentials, antimicrobial applications of metal complexes are the centre of attention for medicinal chemists due to resistance of pathogenic microbes against traditional antibiotics developed from organic synthons [8-10]. Copper was known well for its anti-microbial as well as therapeutic properties from a very long time [11]. Now, its ionic complexes are studied as drugs in modern medical sciences and are of interest among medicinal chemists for evaluating drug likeness behaviour against various lethal diseases [12-16]. In recent years, copper metal ions became very popular along with other transition metal ions for the study of antibacterial properties along with antifungal and anticancer properties of transition metal complexes on both Gram positive and Gram negative bacteria and other microbes and cancer lining cells, respectively [14,17-37]. In the current pandemic of COVID-19, many metal complexes including copper have been tested and found effective against various strains of corona virus by *in silico* mean [12,13]. Transition metal complexes of copper metal ions on a variety of ligands have shown promising results on pathogenic Gram positive bacteria such as *S. aureus, B. subtilis*, *E. Faecalis, S. mutans*, *S. gordonii*, *B. cereus* and Gram-negative bacteria such as *E. coli* and *S. typhi*, *P. aeruginosa* and *K. pneumonia*, *V. cholera* and *S. pneumonia* [17-20]. The final activities of different transition metal complexes of copper ions are different on tested organisms as it largely depends on either the impermeability of cells of organisms or the difference in the ribosome of bacterial cells as well as on the nature of ligands used to prepare the complexes [38-43]. In the present review, we tried to set a view of antibacterial efficacy of copper based metal complexes in front of global researchers to drag their attention for further discoveries and researches to find copper metal complexes as potent antibacterial medicinal agent.

2. Historical Developments for Antibacterials

The treatment of bacterial infections approved by administration of chemotherapeutic agents, the therapy was began in the 1930s, and was one of the most profound medical advances occurred in twentieth century. All the antibacterial drugs in clinics today were developed by drug discovery programmes and systematic studies leads to identify inhibitors by tracing their mode of action and ability to prevent bacterial growth. The 'golden period' of antibacterial-drug discovery was laid between the 1940s and 1970s [44,45]. The development of these therapeutics or agents derived from them helped a lot to combat the disease burden. In the meanwhile the emergence of resistance to antibiotics in pathogenic bacteria worldwide during the past three decades threatened the public health globally and challenged the medicinal chemist profoundly. This could destabilize the major advances achieved in the treatment of infection so far [46-49]. The developments in molecular modelling, bioinformatics, biochemistry and target-based drug discovery program advances the current strategy for finding and develop therapeutics as antibacterial. Though molecular targets for effective antibacterials are fairly few but they are found to involve consistently in the pathways of macromolecular synthesis. They are indeed, the essential components and comprise for functioning of bacteria that cannot be satisfied by providing intermediates. Especially, very few targets of the major classes of antibacterials used in systemic mono-therapy are essential enzymes present in bacterial cell. Some clinical antibacterial drugs used as reference in antibacterial evaluation of metal complexes are listed in Table 1 along with their IUPAC name and chemical structure.

3. Antibacterial Activity of Mononuclear Copper Complexes

Some of the considerable mononuclear copper metal complexes on different ligands were synthesized and screened for their anti-microbial and anti-tumour activities. Transition metal complexes of copper such as $[Cu(L_1)_2]\cdot 2H_2O$, $[Cu(L_2)_2]\cdot 2H_2O$, $[Cu(L_3)_2]\cdot 2H_2O$, $[Cu(L_4)_2]\cdot 2H_2O$ have been prepared by deprotonation of Schiff base ligands (HL_1–HL_4) designed by condensation of 4-Fluorobenzylamine with 2-Hydroxy-1-naphthaldehyde/3,5-Dichlorosalicylaldehyde/3,5-dibromosalicylaldehyde/3-Bromo-5-chlorosalicylaldehyde. All of these metal complexes were characterised using different physiochemical techniques and the spectro analytical data favours well the proposed structure of synthesized ligands and metal complexes [19]. Also *in vitro* screening of these well screened ligands and metal complexes of Cu

Table 1. Chemical structure and IUPAC name of some antibacterial drugs taken as standard/ control during in vitro antibacterial activity screening of ligands and metal complexes.

S.N.	Drug	Chemical structure	IUPAC Name	Ref.
1	Ciprofloxacin	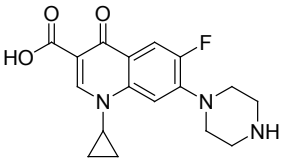	1-Cyclopropyl-6-fluoro-4-oxo-7-piperazin-1-yl-1,4-dihydro-quinoline-3-carboxylic acid	[50]
2	Furacilinum / Furacine	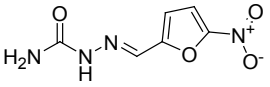	[(E)-(5-nitrofuran-2-yl)methylideneamino]urea	[50]
3	Doxycycline	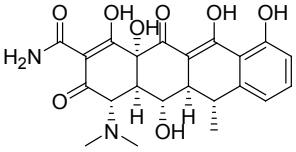	(4S,4aR,5S,5aR,6R,12aR)-4-(dimethylamino)-1,5,10,11,12a-pentahydroxy-6-methyl-3,12-dioxo-4a,5,5a,6-tetrahydro-4H-tetracene-2-carboxamide	[50]
4	Norfloxacin	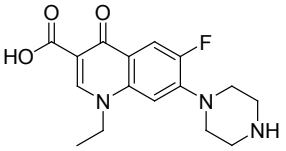	1-ethyl-6-fluoro-4-oxo-7-piperazin-1-ylquinoline-3-carboxylic acid	[50]
5	Ampicillin	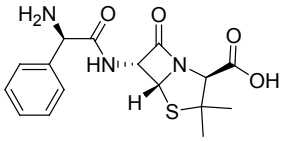	(2S,5R,6R)-6-[[(2R)-2-amino-2-phenylacetyl]amino]-3,3-dimethyl-7-oxo-4-thia-1-azabicyclo[3.2.0]heptane-2-carboxylic acid	[51]
6	Chloramphenicol	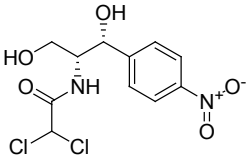	2,2-dichloro-N-[(1R,2R)-1,3-dihydroxy-1-(4-nitrophenyl) propan-2-yl]acetamide	[51]
7	Levofloxacin	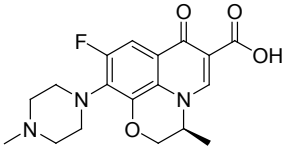	(2S)-7-fluoro-2-methyl-6-(4-methylpiperazin-1-yl)-10-oxo-4-oxa-1-azatricyclo[7.3.1.05,13]trideca-5(13),6,8,11-tetraene-11-carboxylic acid	[50]
8	Streptomycin	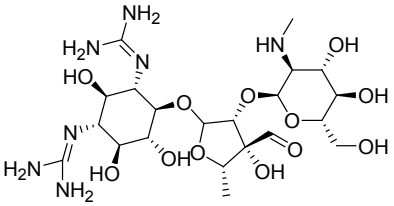	2-[(1R,2R,3S,4R,5R,6S)-3-(diaminomethylideneamino)-4-[(2R,3R,4R,5S)-3-[(2S,3S,4S,5R,6S)-4,5-dihydroxy-6-(hydroxymethyl)-3-(methylamino)oxan-2-yl]oxy-4-formyl-4-hydroxy-5-methyloxolan-2-yl]oxy-2,5,6-trihydroxycyclohexyl]guanidine	[51]
9	Chlorhexidine	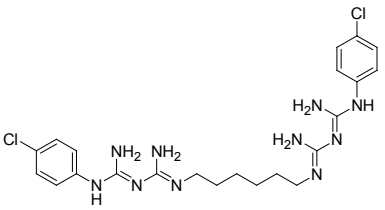	(1E)-2-[6-[[amino-[(E)-[amino-(4-chloroanilino)methylidene] amino]methylidene]amino]hexyl]-1-[amino-(4-chloroanilino) methylidene]guanidine	[50]
10	Gentamycin	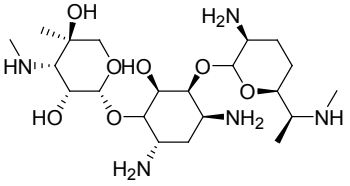	(2R,3R,4S,5R)-2-[(1S,2R,3S,4S,6S)-4,6-diamino-3-[(2S,3S,6S)-3-amino-6-[(1S)-1-(methylamino)ethyl]oxan-2-yl]oxy-2-hydroxycyclohexyl]oxy-5-methyl-4-(methylamino) oxane-3,5-diol	[51]

yielded some fruitful results when tested against Gram positive *S. gordonii and S. aureus* and Gram negative *E. coli* and *P. aeruginosa* with Ciprofloxacin as a standard reference. $[Cu(L_3)_2]\cdot 2H_2O$ showed the most promising results against Gram positive while $[Cu(L_4)_2]\cdot 2H_2O$ showed the most promising result against Gram-negative under laboratory conditions among other metal complexes used in this screening process [19]. Copper complexes of formulae $[Cu(L)_2]\cdot H_2O$, $[Cu(Br)(L)]\cdot H_2O\cdot CH_3OH$, $[Cu(L)Cl]\cdot C_2H_5OH$ of ligand 1-phenyl-3-methyl-4-benzoyl-5-pyrazolone-4-ethylthiosemicarbazone were prepared, purified and screened against Gram positive bacteria *B. cereus* and *S. aureus* and Gram negative *S. abony* using Furacilinum as the standard reference [20]. In results, the metal complexes appeared to be impactful against screened bacteria [20]. Transition metal complex $[Cu(L)_2]$ of crystal X-ray studied ligand 1-(2-nitrobenzylidene)-2-(phthalazin-1-yl)hydrazine was synthesized and characterized by spectral and physical methods viz. IR, UV-vis., NMR, Mass, TGA etc. and then tested for its antibacterial activity against Gram positive *E. faecalis*, *S. mutans* and *S. aureus* and Gram negative *E. coli, P. aeruginosa* and *K. pneumoniae* taking Ciprofloxacin as the standard reference drug and the inhibition capacity of the metal complex, in this case, is accordingly to the inhibition of the ciprofloxacin [18]. Organic ligandsamidino-O-methylurea (L^1), N-(benzyl)-amidino-O-methylurea (L^2), 2,2′-bipyridine (bipy) and 1,10-phenanthroline (phen) were applied to produce a series of mixed ligand copper complexes with formulae $[Cu(L^1)(bipy)].Cl_2$, $[Cu(L^1)(phen)].Cl_2$, $[Cu(L^2)(bipy)Cl_2]$ and $[Cu(L^2)(phen)].Cl_2$ possessing antibacterial properties. Antibacterial potency order of tested complexes were predicted as $[Cu(L^1)(phen)].Cl_2 > [Cu(L^2)(phen)].Cl_2 > [Cu(L^1)(bipy)].Cl_2 > [Cu(L^2)(bipy)Cl_2]$ against three Gram negative bacterial strains E. coli, Salmonella and Campylobacter. The best inhibition action was performed by $[Cu(L^1)(phen)].Cl_2$ against *Campylobactor* [52]. Well characterized copper (I) halide complexes $[Cu(L^1)_2Cl]$, $[Cu(L^1)_2Br]$, $[Cu(L^1)_2I]$, $[Cu(L^2)_2Cl]$, $[Cu(L^2)_2Br]$, $[Cu(L^3)_2Br]$ coordinated with S atoms of thiocarbamide fragments of 4-thioxo[1,3,5] oxadiazocines ligands (L^1- L^3) were evaluated for their antibacterial potential via bioluminescent toxicological assay against E. Coli K12 TG1 bacterial strain and results were compared with free ligands and standard antibacterial drugs Doxycycline, Norfloxacin, Ciprofloxacin, Ampicillin and Chloramphenicol. The complexes of L^1 and L^2 ligands occupied with electron dragging groups showed stronger activity comparable activity to reference drugs against targeted microbial strain [53]. Bioactive Cu(II) mixed ligand complexes [Cu(Lvx)(Dpya)Cl]·Cl and [Cu(Lvx)(Dphen)Cl]·Cl of commercial antibiotic levofloxacin (Lvx) with 2,2′-dipyridylamine (Dpya) and 4,7-Diphenyl-1,10-phenanthroline (DPhen), respectively [Figure 1: i, ii, iii (ligands); Figure 2: 1, 2 (complexes)] were reported active against four Gram positive *S. aureus*, *B. subtilis*, *E. faecalis* and *S. pneumoniae* and five Gram negative *P. mirabilis*, *S. flexneri*, *E. coli*, *Citrobacter* species and *S. typhi* bacterial cells. Antibacterial activity was evaluated *in vitro* by disc diffusion method in agar media as nutrient and results were compared with levofloxacin as parent ligand and neomycin as reference drug. Antimicrobial activity data obtained clearly indicate that inhibition potential of both copper complexes is much higher than the free levofloxacin and metal salt tested against targeted bacterial strains [54]. Methicillin resistant bacteria *S. aureus* and *P. aeruginosa*, *E. coli, M. vaccae, B. subtilis* pathogenic bacterial strains were targeted to evaluate antibacterial efficacy of four novel copper complexes with chiral properties synthesized from terpene derived ethane-1,2-diamine ligand [Figure 1: iv, v, vi, vii (ligands); Figure 2: 3, 4, 5, 6 (complexes)]. Structural elucidation of prepared compounds was done with the help of advance physico spectral techniques and well supported as proposed. IR and NMR data revealed bidentate behaviour of ligands iv-vi, while the ligand viii acts as tridentate in coordination with copper metal ions. The *in vitro* antibacterial potential of all copper complexes was reported comparable to the standard medicine ciprofloxacin used as reference drug [55]. Gram positive *S. aureus*, *B. subtilis* and Gram negative *E. coli*, *S. typhimurium* bacterial strains were targeted by mononuclear complexes (7-14) of acetate, chloride, nitrate, sulphate salts of copper metal ion with a novel hydrazone ligand and/or 8-hydroxyquinoline , 1,10-phenanthroline, benzoylacetone as mixed ligands [Figure 1: viii(H_2L^1), ix(HQ), x(Bac), xi(Phen) ligands; Figure 2: 7, 8, 9, 10, 11, 14 (complexes)]. Antibacterial activity data, in vitro, indicate that the ligand and their metal complexes; $[(HL^1)Cu(OAc)(H_2O)]\cdot 1.5H_2O$ (7), $[(H_2L^1)Cu(SO_4)(H_2O)_2]\cdot 1.5H_2O$ (8), $[(HL^1)Cu(H_2O)_3]\cdot Br\cdot H_2O$ (9), $[(HL^1)Cu(HQ)(H_2O)]$ (10), $[(HL^1)Cu(H_2O)(Bac)]\cdot 2H_2O$ (11) showed a buoyant activity against the Gram positive bacteria; *B. Subtilis*, but complexes $[(HL^1)Cu(H_2O)].NO_3$ (12), $[(HL^1)CuCl]\cdot 1.5H_2O$ (13), $[(HL^1)Cu(OAc)(Phen)]$ (14) showed no effect even. Targeted strains of *S. aureus*, *E. coli*, and *S. typhimurium* were unaffected by test compounds H_2L^1 and all copper complexes [56]. 2-cetylpyridinenicotinichydrazone; HL as ligand applied to synthesize copper complexes as $[Cu(L)_2]$, $[Cu(HL)Cl_2]$ and $[Cu(HL)Br_2]$ in 1:2, 1:1 and 1:1 metal ligand ratio (M : L), respectively. These complexes were well characterized by single X-ray crystallography along with IR, UV-vis., NMR and

Mass spectral techniques. Spectral studies supported well the proposed structure, coordination mode and geometry of copper complexes. These complexes and ligand were studied for the evaluation of in vitro antibacterial potential against *S. mutans, S. mitis, S. sanguinis, S. sobrinus, L. casei, S. salivarius* and *E. faecalis* bacterial strains. Minimum inhibitory concentration of dilutions of ligands and complexes were observed and compared with Chlorhexidine as standard antibacterial drug. The minimum inhibitory concentration data showed the enhanced activity of complexes than free ligand and satisfactory as compared to standard control drug [57].

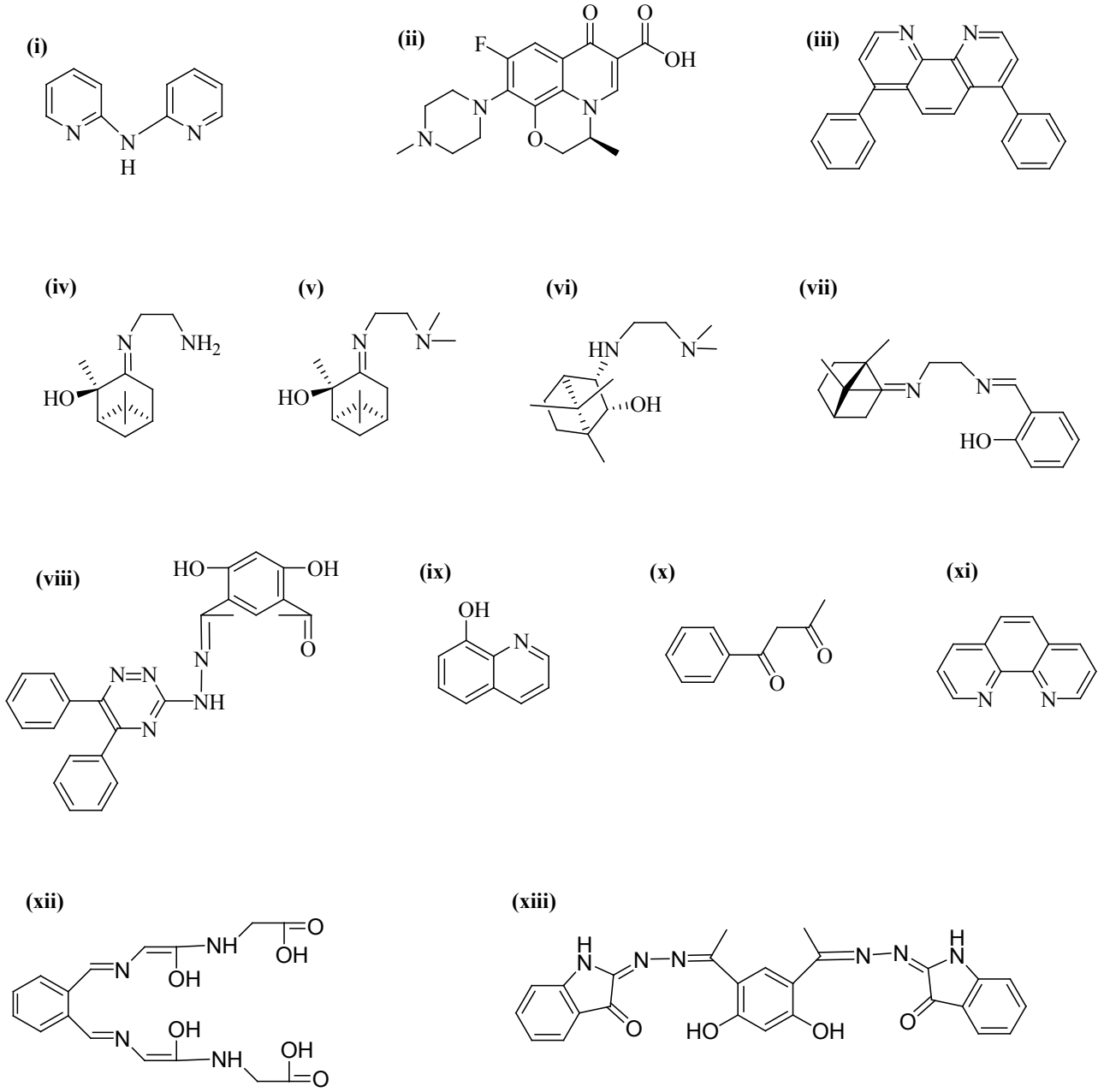

Figure 1. Structure of some antibacterial ligands (i-xiii) applied to prepare copper complexes [53-56]

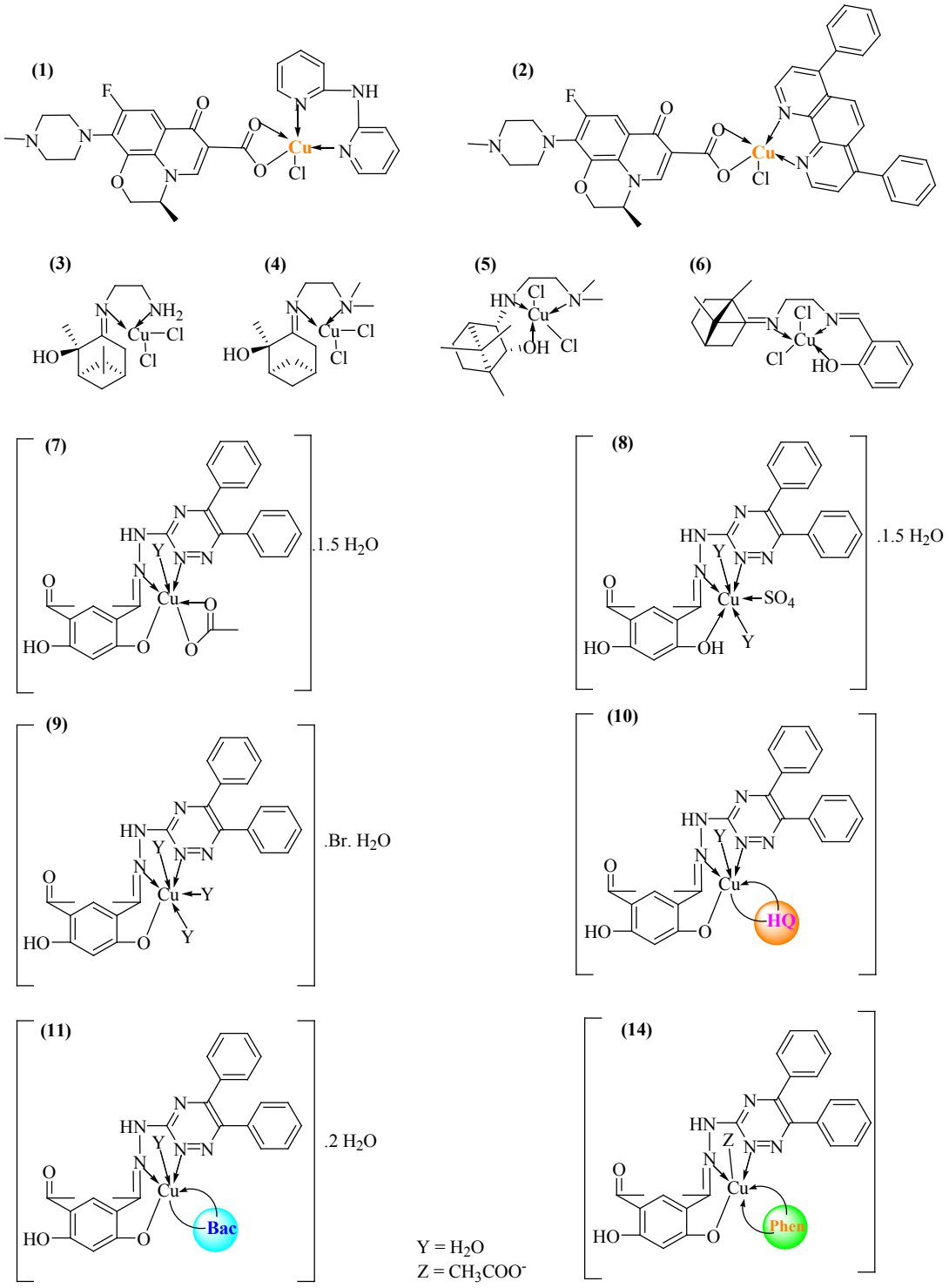

Figure 2. Structure of antibacterial copper complexes (1-11, 14) of ligands (i-vii) [53-56]

4. Antibacterial Activity of Bi-nuclear Copper Complexes

Along with the synthesis of mononuclear metal complexes, a big number of binuclear metal complexes were also synthesized and have been tested for their anti-microbial activities. Transition metal complexes of a copper metal ion such as $[Cu_2(Pym\ L)Cl_3]$ on the Schiff base and Pyrimidine-derivative ligands was synthesized by template condensation of Schiff base (L) derived from glycine using 2,3-butanedione, 5-methyl-2,6-pyrimidine-dione and metal chloride/acetate salt in 1:1:2

stoichiometric ratio [17]. Synthesized compounds were well characterized by its elemental analysis, magnetic measurement and other physiochemical techniques. Tetra dentate coordination behaviour of Schiff base (L) and tridentate behaviour of 5-methyl-2,6-pyrimidine-dione (Pym) was executed by IR and NMR spectral studies. Octahedral environment surroundings of copper metal ions are revealed by UV-visible and EPR spectral studies. These structurally elucidated compounds were then screened for their antibacterial activities by taking Streptomycin as a standard reference against Gram-positive *S. aureus* and *B. subtilis* and Gram-negative *E. coli* and *S. typhi*. The Cu compound showed some excellent result against Gram-positive bacteria and a good result against Gram negative bacteria under laboratory conditions [17]. $[Cu(NO_3)(L)]_2 \cdot C_2H_5OH$ of ligand 1-phenyl-3-methyl-4-benzoyl-5-pyrazolone-4-ethyl-thiosemicarba-zone were prepared, purified and screened against Gram positive bacteria *B. cereus* and *S. aureus* and Gram negative *S. abony* using Furacilinum as the standard reference [21]. In results, the metal complexes appeared to be impactful and showed some excellent results against screened bacteria [21]. Bioactive $[Cu_2(L)(H_2O)_4]$ have been synthesized with a Schiff base ligand derived from diglycine and benzene-1,2-dicarbaldehyde [Figure 1: xii (ligand); Figure 3: 15 (complex)] and evaluated for its *in vitro* antibacterial

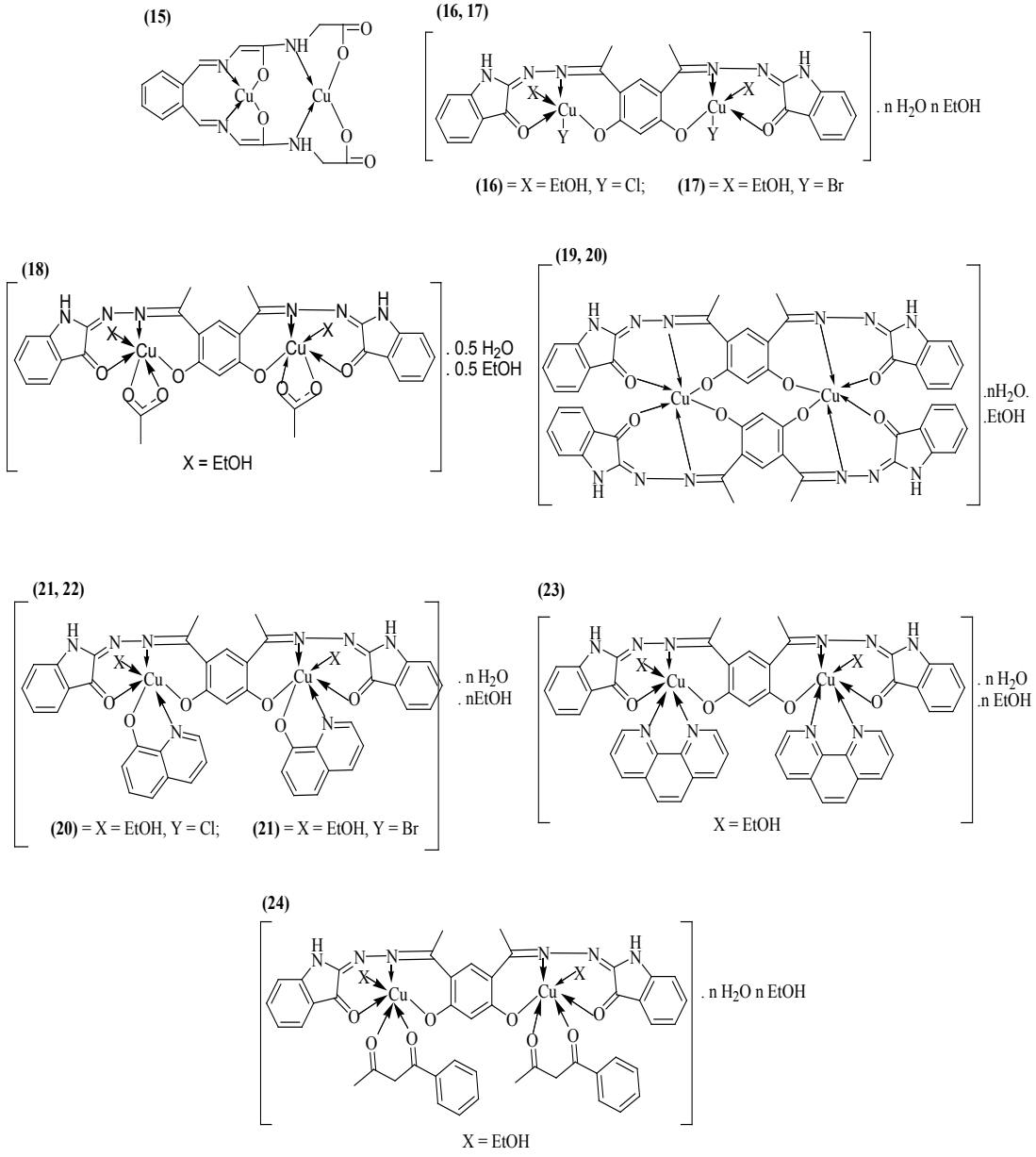

Figure 3. Structure of antibacterial bimetallic copper complexes (15-24) with ligands (xii-xiii) [56-60]

activity at the concentration of 10^3 g/Ml against *B. subtilis and S. aureus, E. coli and K. pneumonia* bacterial strains in the presence of three reference drugs streptomycin, ampicillin and rifampicin. The zone inhibition potential of copper complex was found much improved than free ligand [58]. Deprotonation of a potent ligand, *N*,*N*′-*bis*(*N*-hydroxyethylaminopropyl)oxamido (H_2heap) resulted in the formation of a hydrated binuclear copper complex $[Cu_2(heap)]\cdot(ClO_4)_2\cdot 2H_2O$ on reaction with perchlorate salt of copper metal ion. Bioactivity of complex was evaluated against bacterial strains of *S. aureus, E. coli, B. subtilis* and recorded enhanced antibacterial potential than free ligand *in vitro* [59]. Copper complex of methoxy thiosemicarbazone (MTSC) of formulae $[Cu(MTSC)(NH_3)_3(-Cl)]\cdot 2H_2O$ (12) and $[Cu_2(MTSC)(NH_3)_4(Cl)_2(H_2O)_2]\cdot 2H_2O$ (13) were prepared and tested for their antibacterial potential against *B. subtilis, S. aureus, E. coli and P. vulgaris* with Gentamycin as reference drug. The inhibition potential data indicate that metal complexes have greater potential than free ligand [60]. 4,6-diacetylresorcinol and isatin monohydrazone yielded ligand (H_2L^2) and then allowed to react with Cu^{+2} ion salts in 1:1 and 2:1 stoichiometric ratio resulting bioactive binuclear copper complexes [Figure 1: xii, xiii (ligands); Figure 3: 16-20 (complexes)]. H_2L^2 was further reacted with Cu^{+2} metal ions along with 8-hydroxyquinoline, 1,10-phenanthroline, benzoylacetone to produce mixed ligand binuclear complexes [Figure 1: ix-xi, xiii (ligands); Figure 3: 21-24 (complexes)]. *In vitro* antibacterial activity data assessment divulged that the ligands (H_2L^2) showed activity against *S. aureus*, *B. subtilis* and *E. coli* bacteria. Complexes showed good activity against studied bacteria comparative to free ligand [56].

5. Conclusions

Precisely the transitional metal complexes of copper metal ion can possess antibacterial properties as seen in the different research activities performed by a different group of people around different times. Also, it gives us hope towards achieving new heights in the field of antibacterial drugs. As we have seen during the pandemic of COVID-19, bacterial/fungal co-infections have also raised along with deadly corona virus infections and these co-infections thus increased the mortality rate in corona virus infected patients throughout the globe. The impact of readily available antibiotic drugs getting reduced by many folds because the increasing drug resistance capabilities of the bacteria, these metal complexes based drugs can help us in controlling the damage due to these deadly bacterial infections. These complexes are the hope of future medicinal chemistry as the organic-based drugs are getting ineffective against growing drug resistance of these bacteria. The depth studies of copper coordinated metal complexes based on structural and antibacterial potential along with their synthetic route and mode of action may fulfil the future need of effective antibacterial drug for specified target microbe.

Abbreviations

Acronym	Full word
S. aureus	*Staphylococcus aureus*
B. subtilis	*Bacillus subtilis*
E. Faecalis	*Enterococcus faecalis*
S. mutans	*Streptococcus mutans*
S. gordonii	*Streptococcus gordonii*
B. cereus	*Bacillus cereus*
E. coli	*Escherichia coli*
S. typhi	*Salmonella typhi*
P. aeruginosa	*Pseudomonas aeruginosa*
K. pneumonia	*Klebsiella pneumonia*
V. cholera	*Vibrio cholera*
S. pneumonia	*Streptococcus pneumonia*
S. abony	*Salmonella abony*
P. mirabilis	*Proteus mirabilis*
S. flexneri	*Shigella flexner*
M. Vaccae	*Mycobacterium vaccae*
S. typhimurium	*Salmonella typhimurium*
S. mitis	*Streptococcus mitis*
S. sanguinis	*Streptococcus sanguinis*
S. sobrinus	*Streptococcus sobrinus*
L. casei	*Lacticaseibacillus casei*
S. salivarius	*Streptococcus salivarius*
P. vulgaris	*Proteus vulgaris*

Acknowledgement

Authors are thankful to authorities of Nitishwar Mahavidyalaya (B.R.A. Bihar University), Muzaffarpur for providing the necessary facilities for the write up processing this article. We are also thankful to Dr. S. Mumtazuddin, Professor, Department of Chemistry, B. R. A. Bihar University, Muzaffarpur- India for their valuable suggestions in compilation of data discussed here.

Conflict of Interest

The authors declare no conflict of interest.

References

[1] Makovec, T., 2019. Cisplatin and beyond: molecular mechanisms of action and drug resistance development in cancer chemotherapy. Radiology and Oncol-

ogy. 53(2), 148-158.
DOI: https://dx.doi.org/10.2478%2Fraon-2019-0018

[2] Alderden, R.A., Hall, M.D., Hambley, T.W., 2006. The Discovery and Development of Cisplatin. Journal of Chemical Education. 83(5), 728-734.
DOI: https://doi.org/10.1021/ed083p728

[3] Abu-Dief, A.M., Mohamed, I.M.A., 2015. A review on versatile applications of transition metal complexes incorporating Schiff bases. Beni-Suef University Journal of Basic Applied Science. 4(2), 119-133.
DOI: https://doi.org/10.1016/j.bjbas.2015.05.004

[4] Kawarada, H., Yoshikawa, Y., Yasui, H., et al., 2011. Synthesis and in vitro insulin-mimetic activities of zinc(II) complexes of ethyl 2,5-dihydro-4-hydroxy-5-oxo-1H-pyrrole-3-carboxylates. Metallomics. 3, 675-679.
DOI: https://doi.org/10.1039/C1MT00009H

[5] Mahdavian, M., Attar, M.M., 2009. Electrochemical behaviour of some transition metal acetylacetonate complexes as corrosion inhibitors for mild steel. Corrosion Science. 51(2), 409-414.
DOI: https://doi.org/10.1016/j.corsci.2008.11.010

[6] Chakraborty, J.N., 2011. 13 -Metal-complex dyes, Editor(s): M. Clark, In Woodhead Publishing Series in Textiles, Handbook of Textile and Industrial Dyeing, Woodhead Publishing. 1, 446-465.
DOI: https://doi.org/10.1533/9780857093974.2.446.

[7] Srivastva, A.N., (Ed.), 2017. Stability and Applications of Coordination Compounds. IntechOpen, London.
DOI: https://doi.org/10.5772/intechopen.83186

[8] Srivastava, A.N., Panja, S., Singh, N.P., et al., 2021. Bioactive metal complexes of a Schiff base derived from 2,3-Dioxobutane, Ethane-1,2-diamine and 4-Chloro-2-formylphenol: Spectral studies and *in vitro* antimicrobial activity. Asian Journal of Chemistry. 33(12), 3063-3069.
DOI: https://doi.org/10.14233/ajchem.2021.23478

[9] Jaafar, A., Mansour, N., Fix-Tailler, A., et al., 2022. Synthesis, Characterization, Antibacterial and Antifungal Activities Evaluation of Metal Complexes With Benzaldehyde-4-methylthiosemicarbazone Derivatives. Chemistry Select. 7(10), e202104497.
DOI: https://doi.org/10.1002/slct.202104497

[10] Nandanwar, S.K., Borkar, S.B., Wijaya, B.N., et al., 2020. Cobalt(II) Benzazole Derivative Complexes: Synthesis, Characterization, Antibacterial and Synergistic Activity. Chemistry Select. 5(11), 3471-3476.
DOI: https://doi.org/10.1002/slct.202000222

[11] Jones, C.J., Thornback, J.R., 2007. Medicinal Applications of Coordination Chemistry. The Royal Society of Chemistry, Cambridge, U.K.
DOI: https://doi.org/10.1039/9781847557759

[12] Kumar, S., Choudhary, M., 2022. Synthesis and characterization of novel copper(II) complexes as potential drug candidates against SARS-CoV-2 main protease. New Journal of Chemistry. 46, 4911-4926.
DOI: https://doi.org/10.1039/D2NJ00283C

[13] Ali, A., Sepay, N., Afzal, M., et al., 2021. Molecular designing, crystal structure determination and in silico screening of copper(II) complexes bearing 8-hydroxyquinoline derivatives as anti-COVID-19. Bioorganic Chemistry. 110, 104772.
DOI: https://doi.org/10.1016/j.bioorg.2021.104772

[14] Yousuf, I., Bashir, M., Arjmand, F., et al., 2021. Advancement of metal compounds as therapeutic and diagnostic metallodrugs: Current frontiers and future perspectives. Coordination Chemistry Review. 445, 214104.
DOI: https://doi.org/10.1016/j.ccr.2021.214104

[15] Yousuf, S., Arjmand, F., Tabassum, S., 2021. Design, synthesis, ligand's scaffold variation and structure elucidation of Cu(II) complexes; In vitro DNA binding, morphological studies and their anticancer activity. Polyhedron. 209, 115450.
DOI: https://doi.org/10.1016/j.poly.2021.115450.

[16] Pelosi, G., Bisceglie, F., Bignami, F., et al., 2010. Antiretroviral activity of thiosemicarbazone metal complexes. Journal of Medicinal Chemistry. 53(24), 8765-8769.
DOI: https://doi.org/10.1021/jm1007616

[17] Srivastva, A.N., Singh, N.P., Shriwastaw, C.K., 2016. In vitro antibacterial and antifungal activities of binuclear transition metal complexes of ONNO Schiff base and 5-methyl-2,6-pyrimidine-dione and their spectroscopic validation. Arabian Journal of Chemistry. 9, 48-61.
DOI: https://doi.org/10.1016/j.arabjc.2014.10.004

[18] Bakale, R.P., Naik, G.N., Machakanur, S.S., et al., 2018. Structural characterization and antimicrobial activities of transition metal complexes of a hydrazone ligand. Journal of Molecular Structure. 1154, 92-99.
DOI: https://doi.org/10.1016/j.molstruc.2017.10.035

[19] Devi, J., Yadav, M., Kumar, D., et al., 2019. Some divalent metal(II) complexes of salicylaldehyde-derived Schiff bases: Synthesis, spectroscopic characterization, antimicrobial and in vitro anticancer studies. Appllied Organometallic Chemistry. 33, e4693.
DOI: https://doi.org/10.1002/aoc.4693

[20] Hazra, M., Dolai, T., Pandey, A., et al., 2014. Synthesis and Characterisation of Copper(II) Complexes

with Tridentate NNO Functionalized Ligand: Density Function Theory Study, DNA Binding Mechanism, Optical Properties, and Biological Application. Bioinorgnic Chemistry and Applications. 1-13.
DOI: https://doi.org/10.1155/2014/104046

[21] Pahontu, E., Julea, F., Rosu, T., et al., 2015. Antibacterial, antifungal and in vitro antileukemia activity of metal complexes with thiosemicarbazones. Journal of Cellular and Molecular Medicine. 19, 865-878.
DOI: https://doi.org/10.1111/jcmm.12508

[22] Mishra, A.P., Mishra, R., Jain, R., et al., 2012. Synthesis of New VO(II), Co(II), Ni(II) and Cu(II) Complexes with Isatin-3-Chloro-4-Floroaniline and 2-Pyridinecarboxylidene-4-Aminoantipyrine and their Antimicrobial Studies. Mycobiology. 40, 20-26.
DOI: https://doi.org/10.5941/MYCO.2012.40.1.020

[23] Kathiresan, S., Anand, T., Mugesh, S., et al., 2015. Synthesis, spectral characterization and DNA bindings of tridentate N_2O donor Schiff base metal(II) complexes. Journal of Photochemistry and Photobiology B: Biology. 148, 290-301.
DOI: https://doi.org/10.1016/j.jphotobiol.2015.04.016

[24] Karekal, M.R., Biradar, V., Bennikallu Hire Mathada, M., 2013. Synthesis, Characterization, Antimicrobial, DNA Cleavage, and Antioxidant Studies of Some Metal Complexes Derived from Schiff Base Containing Indole and Quinoline Moieties. Bioinorgnic Chemistry and Applications. 1-16.
DOI: https://doi.org/10.1155/2013/315972

[25] Raman, N., Sakthivel, A., Pravin, N., 2014. Exploring DNA binding and nucleolytic activity of few 4-amino -antipyrine based amino acid Schiff base complexes: A comparative approach. Spectrochimica Acta Part A: Molecular and Biomolecular Spectroscopy. 125, 404-413.
DOI: https://doi.org/10.1016/j.saa.2014.01.108

[26] Mahmoud, W.H., Mohamed, G.G., El-Sayed, O.Y., 2018. Coordination compounds of some transition metal ions with new Schiff base ligand derived from dibenzoyl methane. Structural characterization, thermal behavior, molecular structure, antimicrobial, anticancer activity and molecular docking studies. Appllied Organometallic Chemistry. 32, e4051.
DOI: https://doi.org/10.1002/aoc.4051

[27] Chohan, Z.H., Supuran, C.T., 2005. Organometallic compounds with biologically active molecules: *in vitro* antibacterial and antifungal activity of some 1,1′-(dicarbohydrazono) ferrocenes and their cobalt(II), copper(II), nickel(II) and zinc(II) complexes. Appllied Organometallic Chemistry. 19, 1207-1214.
DOI: https://doi.org/10.1002/aoc.944

[28] Alagha, A., Parthasarathi, L., Gaynor, D., et al., 2011. Metal complexes of cyclic hydroxamates. Synthesis and crystal structures of 3-hydroxy-2-methyl-3H-quinazolin-4-one (CHaH) and of its Fe(III), Co(II), Ni(II), Cu(II) and Zn(II) complexes. Inorganica Chimica Acta. 368, 58-66.
DOI: https://doi.org/10.1016/j.ica.2010.12.047

[29] Nandanwar, S.K., Kim, H.J., 2019. Anticancer and Antibacterial Activity of Transition Metal Complexes. Chemistry Select. 4, 1706-1721.
DOI: https://doi.org/10.1002/slct.201803073

[30] Psomas, G., Kessissoglou, D.P., 2013. Quinolones and non-steroidal anti-inflammatory drugs interacting with copper(II), nickel(II), cobalt(II) and zinc(II): structural features, biological evaluation and perspectives. Dalton Transactions. 42, 6252-6276.
DOI: https://doi.org/10.1039/C3DT50268F

[31] Nagender, P., Kumar, R.N., Reddy, G.M., et al., 2016. Synthesis of novel hydrazone and azole functionalized pyrazolo[3,4-*b*]pyridine derivatives as promising anticancer agents. Bioorganic and Medicinal Chemistry Letters. 26, 4427-4432.
DOI: https://doi.org/10.1016/j.bmcl.2016.08.006

[32] Arbaoui, A., Redshaw, C., Sanchez-Ballester, N.M., et al., 2011. Bimetallic copper(II) and zinc(II)complexes of acrylic Schiff base ligands derived from amino acids. Inorganica Chimica Acta. 365, 96-102.
DOI: https://doi.org/10.1016/j.ica.2010.08.043

[33] Kumar, G., Kumar, D., Devi, S., et al., 2010. Synthesis, spectral characterization and antimicrobial evaluation of Schiff base Cu(II), Ni(II) and Co(II) complexes. European Journal of Medicinal Chemistry. 45, 3056-3062.
DOI: https://doi.org/10.1016/j.ejmech.2010.03.036

[34] Singh, N.P., Srivastava, A.N., 2012. Physico-chemical and biological studies of Cu(II), Co(II) and Ni(II) complexes of an N4 coordinating ligand derived from the Schiff base of diacetyl with ethylenediamine and benzoic acid. Journal of Serbian Chemical Society. 77, 627-637.
DOI: https://doi.org/10.2298/JSC110412148S

[35] Chityala, V.K., Kumar, K.S., Subhashini, N.J.P., et al., 2013. Synthesis, crystal structure, spectroscopic, and biological studies on Cu(II) complexes of N_2O donor dimethyl isoxazole Schiff bases. Journal of Coordination Chemistry. 66, 274-286.
DOI: https://doi.org/10.1080/00958972.2012.755174

[36] Gamba, I., Mutikainen, I., Bouwman, E., et al., 2013. Synthesis and characterization of copper complexes of a tetrapyridyl ligand, and their use in the catalytic aerobic oxidation of benzyl alcohol. European Jour-

nal of Inorganic Chemistry. 115-123.
DOI: https://doi.org/10.1002/ejic.201200807

[37] Evangelinou, O., Hatzidimitriou, A.G., Velali, E., et al., 2014. Mixed-ligand copper(I) halide complexes bearing 4,5-bis(diphenylphosphano)-9,9-dimethyl-xanthene and *N*-methylbenzothiazole-2-thione: Synthesis, structures, luminescence and antibacterial activity mediated by DNA and membrane damage. Polyhedron. 72, 122-129.
DOI: https://doi.org/10.1016/j.poly.2014.02.002

[38] Singh, K., Barwa, M.S., Tyagi, P., 2066. Synthesis, characterization and biological studies of Co (II), Ni (II), Cu (II) and Zn (II) complexes with bidentate Schiff bases derived by heterocyclic ketone. European Journal of Medicinal Chemistry. 41, 147-153.
DOI: https://doi.org/10.1016/j.ejmech.2005.06.006

[39] Tabassum, S., Asim, A., Arjmand, F., et al., 2012. Synthesis and characterization of copper(II) and zinc(II)-based potential chemotherapeutic compounds: their biological evaluation viz. DNA binding profile, cleavage and antimicrobial activity. European Journal of Medicinal Chemistry. 58, 308-316.
DOI: https://doi.org/10.1016/j.ejmech.2012.09.051

[40] Srivastva, A.N., Singh, N.P., Shriwastaw, C.K., 2017. De novo synthesis of trivalent metal complexes with ligand derived from N1-[2-(2-Amino-ethylimino)-1-methyl-propylidene]-ethane-1,2- diamine and 4-chloro benzoic acid: spectroscopic validation and in vitro biological studies. Research on Chemical Intermediates. 43, 3663-3675.
DOI: https://doi.org/10.1007/s11164-016-2839-6

[41] Lippard, S.J., Berg, J.M., 1994. Principles of Bioinorganic Chemistry, *University Science Books,* Mill Valley, CA.
DOI: https://doi.org/10.1016/0307-4412(95)90685-1

[42] Parveen, S., Arjmand, F., Zhang, Q., et al., 2020. Molecular docking, DFT and antimicrobial studies of Cu (II) complex as topoisomerase I inhibitor. Journal of Biomolecular Structure and Dynamics. 25, 1-14.
DOI: https://doi.org/10.1080/07391102.2020.1743365

[43] Zehra, S., Tabassum, S., Arjmand, F., 2021. Biochemical pathways of copper complexes: progress over the past 5 years. Drug Discovery Today. 26(4), 1086-1096.
DOI: https://doi.org/10.1016/j.drudis.2021.01.015

[44] Chopra, I., Hesse, L., O'Neill, A.J., 2022. Exploiting current understanding of antibiotic action for discovery of new drugs. Journal of Applied Microbiology. 92, 4S-15S.
DOI: https://doi.org/10.1046/j.1365-2672.92.5s1.13.x

[45] Knowles, D.J.C., 1997. New strategies for antibacterial drug design. Trends in Microbiology. 5, 379-383.
DOI: https://doi.org/10.1016/S0966-842X(97)01128-1

[46] Payne, D.J., Gwynn, M.N., Holmes, D.J., et al., 2007. Drugs for bad bugs: confronting the challenges of antibacterial discovery. Nature Review Drug Discovery. 6, 29-40.
DOI: https://doi.org/10.1038/nrd2201

[47] Spellberg, B., Guidos, R., Gilbert, D., et al., 2008. The epidemic of antibiotic-resistant infections: a call to action for the medical community from the Infectious Diseases Society of America. Clinical Infectious Diseases. 46, 155-164.
DOI: https://doi.org/10.1086/524891

[48] Talbot, G.H., Bradley, J., Edwards(Jr.), J.E., et al., 2006. Bad bugs need drugs: an update on the development pipeline from the Antimicrobial Availability Task Force of the Infectious Diseases Society of America. Clinical Infectious Diseases. 42, 657-668.
DOI: https://doi.org/10.1086/503200

[49] Newman, D.J., Cragg, G.M., Snader, K.M., 2000. The influence of natural products upon drug discovery. Natural Product Reports. 17, 215-234.
DOI: https://doi.org/10.1039/A902202C

[50] National Center for Biotechnology Information, 2022. PubChem Compound Summary. https://pubchem.ncbi.nlm.nih.gov/.

[51] Kar, A., 2005. Medicinal Chemistry (3rd Ed.), New Age International Publishers, New Delhi, India. pp. 629-671.

[52] Meenongwa, A., Brissos, R.F., Soikum, C., et al., 2016. Effects of N, N-heterocyclic ligands on the in vitro cytotoxicity and DNA interactions of copper (II) chloride complexes from amidino-O-methylurea ligands. New Journal of Chemistry. 40(7), 5861-5876.
DOI: https://doi.org/10.1039/C5NJ03439F

[53] Kuzovlev, A.S., Volkova, D.A., Parfenova, I.V., et al., 2020. (i) halide and palladium (ii) chloride complexes of 4-thioxo [1, 3, 5] oxadiazocines: synthesis, structure and antibacterial activity. New Journal of Chemistry. 44(19), 7865-7875.
DOI: https://doi.org/10.1039/C9NJ05958J

[54] Kumar, M., Kumar, G., Dadure, K.M., et al., 2019. Copper (II) complexes based on levofloxacin and 2N-donor ligands: synthesis, crystal structures and in vitro biological evaluation. New Journal of Chemistry. 43(38), 15462-15481.
DOI: https://doi.org/10.1039/C9NJ03178B

[55] Gur'eva, Y.A., Zalevskaya, O.A., Shevchenko, O.G., et al., 2022. Copper (ii) complexes with terpene derivatives of ethylenediamine: synthesis, and antibacterial, antifungal and antioxidant activity. RSC

Advances. 12(15), 8841-8851.
DOI: https://doi.org/10.1039/D2RA00223J

[56] Shebl, M., El-ghamry, M.A., Khalil, S.M.E., et al., 2014. Mono- and binuclear copper(II) complexes of new hydrazone ligands derived from 4,6-diacetylresorcinol: Synthesis, spectral studies and antimicrobial activity. Spectrochimica Acta Part A: Molecular and Biomolecular Spectroscopy. 126, 232-241.
DOI: https://doi.org/10.1016/j.saa.2014.02.014

[57] Santiago, P.H.O., Santiago, M.B., Martins, C.H.G., et al., 2020. Copper(II) and zinc(II) complexes with Hydrazone: Synthesis, crystal structure, Hirshfeld surface and antibacterial activity. Inorganica Chimica Acta. 508, 119632.
DOI: https://doi.org/10.1016/j.ica.2020.119632

[58] Geeta, B., Shravankumar, K., Muralidhar Reddy, P., et al., 2010. Binuclear cobalt(II), nickel(II), copper(II) and palladium(II) complexes of a new Schiff-base as ligand: Synthesis, structural characterization, and antibacterial activity. Spectrochimica Acta Part A: Molecular and Biomolecular Spectroscopy. 77(4), 911-915.
DOI: https://doi.org/10.1016/j.saa.2010.08.004

[59] Zhu, C.Y., Li, Y.T., Wu, Z.Y., et al., 2007. Synthesis, crystal structure and antibacterial activity of a new binuclear copper(II) complex with *N* , *N* ′- *bis* (*N* -hydroxyethylaminopropyl)oxamido as a bridging ligand. Journal of Coordination Chemistry. 60(4), 465-472.
DOI: https://doi.org/10.1080/00958970600880831

[60] Gaber, A., Refat, M.S., Belal, A.A., et al., 2021. New Mononuclear and Binuclear Cu(II), Co(II), Ni(II), and Zn(II) Thiosemicarbazone complexes with potential biological activity: Antimicrobial and molecular docking study. Molecules. 26(8), 2288.
DOI: https://doi.org/10.3390/molecules26082288

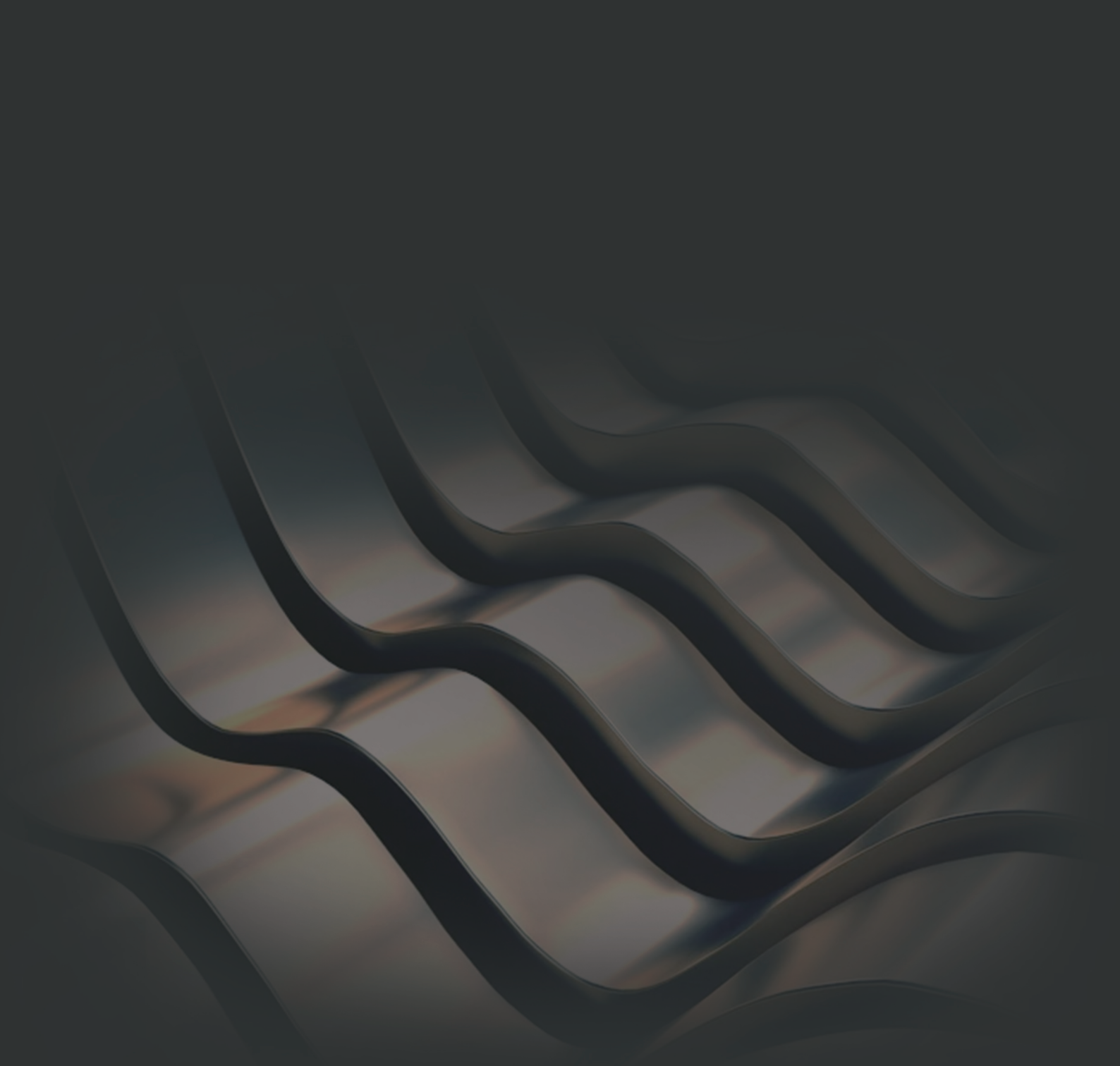

BILINGUAL
PUBLISHING CO.
Pioneer of Global Academics Since 1984

Tel.:+65 65881289
E-mail: contact@bilpublishing.com
Website:ojs.bilpublishing.com

2630-5135 02
9 772630 513229